# WITHDRAWN: Cardiomyocyte βII Spectrin Plays a Critical Role in Maintaining Cardiac Function via Regulating Mitochondrial Respiratory Function

**Shan Wang**

wangshan19840163.com

Fourth Military Medical University

**Rongjin Yang**

Xijing Hospital, Air Force Medical University

**Banjun Ruan**

Xijing Hospital, Air Force Medical University

**Rutao Wang**

Xijing Hospital, Air Force Medical University

**Xiaomeng Zhang**

Xijing Hospital, Air Force Medical University

**Pingping Xing**

Xijing Hospital, Air Force Medical University

**Congye Li**

Xijing Hospital

**Yunyun Zhang**

Xijing Hospital, Air Force Medical University

**Xiaoqian Chang**

Xijing Hospital

**Shun Zhang**

Xijing Hospital, Air Force Medical University

**Huishao Zhao**

Xijing Hospital, Fourth Military Medical University

**Feiyu Zhang**

Xijing Hospital, Air Force Medical University

**Tao Yin**

Xijing Hospital, the Fourth Military Medical University

**Tingting Qi**

Xijing Hospital

**Wenjun Yan**

Xijing Hospital
**Fuyang Zhang**
xijing hospital, fourth military medical university https://orcid.org/0000-0002-6335-9809
**Guangyu Hu**
xijing hospital, fourth military medical university https://orcid.org/0000-0002-9091-4484
**Ling Tao**
Xijing Hospital

**Article**

**Keywords:** βII spectrin, Cardiac function, Mitochondria, Cytoskeleton, Mitochondrial complex I

**Posted Date:** September 20th, 2022

**DOI:** https://doi.org/10.21203/rs.3.rs-2051741/v1



**Additional Declarations:** There is **NO** Competing Interest.

## EDITORIAL NOTE:

The full text of this preprint has been withdrawn by the authors while they make corrections to the work. Therefore, the authors do not wish this work to be cited as a reference. Questions should be directed to the corresponding author.

# Abstract

βII spectrin is a cytoskeletal protein known to be tightly linked to heart development and cardiovascular electrophysiology. However, roles of βII spectrin in cardiac contractile function and post-myocardial infarction pathological remodeling remain unclear. Here, we uncovered that the levels of serum βII spectrin breakdown products (βII SBDPs) were significantly increased in patients with acute myocardial infarction. Consistently, βII spectrin was degraded into βII SBDPs by calpain in mouse hearts after ischemia/reperfusion (I/R) injury. Cardiac-specific βII spectrin deletion results in spontaneous development of cardiac contractile dysfunction, cardiac hypertrophy and fibrosis. Moreover, deletion of βII spectrin in the adult heart exacerbated I/R-induced cardiomyocyte death and heart failure, while restoration of βII spectrin expression by adenoviral saRNA delivery in the heart reduced I/R injury. IP–LC–MS/MS and functional studies revealed that βII spectrin is indispensable for mitochondrial complex I activity and respiratory function. Mechanistically, βII spectrin interacted with mitochondrial complex I to mediate its assembly by crosslinking with actin filaments (F-actin) to maintain F-actin stability. These findings identify βII spectrin as an essential mitochondrial cytoskeletal element for preserving mitochondrial homeostasis and cardiac function.


# Introduction

The cytoskeleton is a complex and highly dynamic network of protein filaments, such as microtubules, actin filaments, and intermediate filaments[1]. The functional roles of the cytoskeleton are to impart mechanical strength, allow intracellular transport and spatial organization, connect the cell to its environment, and generate forces that permit movement[2]. Many cytoskeletal elements play crucial roles in regulating the structural and functional organization of organelles. However, the cytoskeleton component that regulates specific organelles in cardiomyocytes and plays indispensable roles in cardiac physiology and pathophysiology remains to be identified.

Spectrin is a large, cytoskeletal protein that was first discovered in erythrocytes and is important for maintaining the stability, structure, and shape of the cell membrane[3, 4]. The spectrin meshwork is formed by heterodimeric units of α- and β-spectrin assembled side-to-side in an antiparallel fashion, which then form head-to-head tetramers that interact with both the actin cytoskeleton and various membrane proteins via scaffolding proteins, such as ankyrins or 4.1 proteins[5, 6, 7]. Although the critical role of spectrin in erythrocytic structure and function is well recognized, much less is known regarding its function in cardiomyocytes. The spectrin superfamily is composed of seven genes, with two encoding α-spectrins (αI and αII) and five encoding β-spectrins (βI through βV)[7]. βII spectrin, encoded by SPTBN1, is the most common isoform of non-erythrocytic spectrin and is expressed in the heart[8]. Loss of βII spectrin in mice prevents cardiomyocyte differentiation and heart development[9, 10]. βII spectrin levels are altered in acquired forms of human heart failure, as well as in animal models of heart failure, suggesting a role of βII spectrin in cardiac pathology[11]. In addition, a recent study demonstrated that conditional deletion of βII spectrin in the heart results in ventricular arrhythmia[12]. However, whether βII spectrin is required in

maintaining normal cardiac contractile function is unclear. Moreover, role of βII spectrin in post-myocardial infarction pathological remodeling, a critical challenge in cardiac clinical practice, remains unknown. Finally, subcellular and molecular mechanisms responsible for spectrin-related cardiac regulation have not been identified.

Thus, the aims of this study were to clarify the roles of βII spectrin in maintaining physiological cardiac function and post-ischemic pathological remodeling and to determine the responsible mechanisms.

# Results

### Serum βII SBDPs levels are increased in patients with AMI

Previous studies have shown that αII and βII spectrin are degraded into breakdown products (spectrin breakdown products, SBDPs) in the brain after traumatic and ischemic brain injuries, and these SBDPs can be detected in the cerebrospinal fluid[13, 14, 15]. To investigate whether βII spectrin is involved in ischemic heart injury, we first assessed the association of serum βII SBDPs with acute myocardial infarction (AMI). We observed that βII SBDPs were readily detectable in the serum of patients with AMI via immunoblotting (Fig. 1a). Moreover, we enrolled 42 consecutive AMI patients and 64 consecutive non-obstructive coronary artery disease (NOCAD, defined as stenosis <50% of the coronary artery diameter[16]) patients to detect serum βII SBDPs levels via ELISA. We observed that serum βII SBDPs levels were significantly higher in AMI patients than in NOCAD patients (Fig. 1b). These findings indicate that serum βII SBDPs levels are significantly increased in AMI patients.

### βII spectrin protein is degraded by calpain in the heart after I/R injury

Next, we examined the expression of βII spectrin at different time points in mouse hearts during I/R injury. We found that βII spectrin protein expression was significantly decreased in ischemic hearts after 3 h and 6 h of reperfusion (Fig. 1c, d). However, there were no significant differences in cardiac βII spectrin mRNA levels during I/R injury (Fig. 1e). Consistent with these results, the protein levels of βII spectrin in mouse neonatal cardiomyocytes (NCMs) were significantly reduced after hypoxia/ reoxygenation (H/R) (Fig. 1f, g), while the mRNA levels of βII spectrin remained unchanged (Fig. 1h). These results suggest that βII spectrin protein levels are regulated by posttranslational mechanisms.

Several studies have revealed that calpain plays a vital role in I/R injury[17, 18, 19]. Given that spectrins are calpain substrates[15, 20], we hypothesized that βII spectrin degradation might be mediated by calpain. We subjected NCMs to H/R in the presence or absence of the calpain inhibitor T2470. We found that βII spectrin was significantly degraded into multiple βII SBDPs, while the calpain inhibitor significantly attenuated βII spectrin degradation under H/R conditions (Fig. 1i, j). Collectively, these data suggest that βII spectrin is degraded by calpain in the heart after I/R injury.

### βII spectrin deletion in the adult heart results in spontaneous development of contractile dysfunction, cardiac hypertrophy and fibrosis

To evaluate the role of βII spectrin in cardiac physiology and disease, we generated adult cardiac-specific βII spectrin deletion (βII spectrin cKO) mice. βII spectrin$^{flox/flox}$ mice were crossed with tamoxifen-inducible αMHC-CreERT2 mice to generate αMHC-CreERT2-βII spectrin$^{flox/flox}$ mice (Supplementary Fig. 1a*)*. Adult male αMHC-CreERT2-βII spectrin$^{flox/flox}$ mice were treated with tamoxifen for 7 consecutive days to induce cardiac-specific deletion of βII spectrin, and mixed cohorts of βII spectrin$^{flox/flox}$ Cre− and αMHC-Cre+ littermates treated with tamoxifen were used as controls. Immunoblot analysis confirmed the absence of βII spectrin protein in the hearts of βII spectrin cKO mice 1-week post-tamoxifen treatment (Supplementary Fig. 1b, g). However, βII spectrin expression in the brain, liver, kidney, and skeletal muscle was unchanged (Supplementary Fig. 1c–g). No significant cardiac dysfunction was observed at this early time point (Fig. 2a–e). However, 5 weeks post-tamoxifen treatment, we observed a significant decrease in cardiac contractile function, as indicated by a decreased left ventricular ejection fraction (LVEF), decreased left ventricular fractional shortening (LVFS), and increased left ventricular end-systolic diameter (LVESD) and left ventricular end-diastolic diameter (LVEDD), in βII spectrin cKO mice compared to control mice (Fig. 2a–e). In addition, βII spectrin cKO mice displayed cardiac hypertrophy, as evidenced by the greater myocyte cross-sectional area (Fig. 2f, g) and the greater heart weight adjusted for body weight (Fig. 2h) in βII spectrin cKO mice than in control mice. Furthermore, histopathological analysis revealed that βII spectrin cKO mice had markedly more interstitial fibrosis than control mice, as indicated by Masson's trichrome staining (Fig. 2i, j). Additionally, after 8 weeks of tamoxifen induction, βII spectrin cKO mice presented significantly reduced viability (Fig. 2k). These data demonstrate that cardiac-specific βII spectrin deletion in adult mice results in cardiac contractile dysfunction, cardiac hypertrophy and fibrosis without pathological stress.

### βII spectrin deletion in the adult heart exacerbates cardiac I/R injury

Having demonstrated the role of βII spectrin in maintaining physiological cardiac contractile function, we next determined its role in cardiac I/R injury. Adult cardiac-specific βII spectrin deletion mice were subjected to I/R surgery or a sham operation one-week post-tamoxifen treatment, a time point at which spontaneous cardiac dysfunction has not developed in cardiac-specific βII spectrin-deficient mice. We first evaluated cardiac function via echocardiography 1 day post-I/R. Compared with the corresponding sham mice, both βII spectrin cKO and control mice subjected to I/R had notably decreased cardiac contractile function, as indicated by decreases in LVEF and LVFS and increases in LVESD and LVEDD (Fig. 3a–e). Importantly, cardiac-specific βII spectrin deficiency significantly aggravated I/R-induced cardiac contractile dysfunction (Fig. 3a–e). Evans blue and triphenyltetrazolium chloride (TTC) staining further revealed that cardiac-specific βII spectrin deficiency markedly elevated the I/R-induced myocardial infarct size (Fig. 3f–h). Moreover, cardiac-specific βII spectrin deficiency increased I/R-induced myocardial necrosis, as evidenced by elevations in lactate dehydrogenase (LDH) and creatine kinase-MB (CK-MB) release (Fig. 3i, j). Finally, cardiac-specific βII spectrin deficiency increased the number of terminal deoxyribonucleotidyl transferase dUTP nick-end labeling (TUNEL)-positive cells (Fig. 3k, l) in the left ventricular infarct area, which indicated increased apoptosis. To determine the sustained effect of βII spectrin deficiency on post-MI remodeling, we assessed long-term cardiac function and remodeling at day

28 after I/R. Cardiac-specific βII spectrin deficiency exacerbated I/R-induced cardiac contractile dysfunction (Fig. 3m, n) and myocardial fibrosis (Fig. 3o, p).

To complement our in vivo findings, we isolated NCMs and then infected them with adenoviruses expressing short hairpin RNA (shRNA) sequences targeting βII spectrin or a control sh-scramble sequence. The shRNA construct effectively knocked down βII spectrin protein expression (Supplementary Fig. 2a, b). A Cell Counting Kit-8 (CCK-8) assay showed that βII spectrin knockdown significantly reduced NCM viability under H/R conditions (Supplementary Fig. 2c). Furthermore, βII spectrin knockdown in NCMs increased the H/R-induced expression of cleaved caspase-3 (Supplementary Fig. 2d, e) and apoptosis (Supplementary Fig. 2f–i).

Overall, these data demonstrate that defects in βII spectrin are critical for I/R-induced cardiomyocyte death, the sequelae of adverse cardiac remodeling, and heart failure.

### Cardiac-specific loss of βII spectrin impairs mitochondrial complex I activity and respiratory function

To understand the subcellular and molecular mechanisms of βII spectrin in cardiomyocyte function in an unbiased fashion, we employed immunoprecipitation coupled with mass spectrometry (IP–LC–MS/MS) to identify potential βII spectrin binding partners endogenously using a specific antibody against βII spectrin in NCMs. Then, we performed Gene Ontology and KEGG pathway enrichment analyses of the potential βII spectrin binding partners. The design of the experiments is shown in Fig. 4a. For the “subcellular localization” ontology, the top three enriched categories were cytoplasm, membrane and mitochondrion (Fig. 4b). In addition, KEGG pathway analysis revealed an enrichment of proteins functioning in mitochondrial damage-associated neurodegenerative diseases and mitochondrial metabolism, especially oxidative phosphorylation (Fig. 4c). These data suggest that βII spectrin is closely related to mitochondrial function. Therefore, we examined myocardial mitochondrial morphology with transmission electron microscopy (TEM) in βII spectrin cKO and control mice 5 weeks post-tamoxifen treatment. We found that cardiac-specific βII spectrin deficiency provoked mitochondrial morphological abnormalities, as indicated by greater swelling, a decreased number of mitochondrial cristae and reduced cristae areas (Fig. 4d–g). We also tested the mitochondrial membrane potential via JC-1 staining and found that βII spectrin knockdown significantly decreased the mitochondrial membrane potential in NCMs (Fig. 4h, i). Moreover, we used a MitoSOX-based flow cytometry assay to assess mitochondrial reactive oxygen species (ROS) levels and found that βII spectrin knockdown increased mitochondrial ROS production in NCMs (Fig. 4j, k). In addition, we conducted enzyme activity assays for each mitochondrial electron transport chain (ETC) complex and found that βII spectrin knockdown in NCMs significantly decreased the activity of ETC complex I (Fig. 4l). There was no significant difference in ETC complex II, III or IV activity between control and βII spectrin knockdown NCMs (Fig. 4m–o). Moreover, βII spectrin knockdown inhibited ATP production in NCMs (Fig. 4p). We further determined the effect of βII spectrin on mitochondrial respiratory capacity by measuring the oxygen consumption rate (OCR). As expected, βII spectrin knockdown significantly suppressed parameters related to mitochondrial respiratory capacity, including basal respiration, ATP production, maximal respiration and spare respiration, in NCMs (Fig. 4q,

r). Taken together, these data demonstrate that defects in βII spectrin impair mitochondrial structure, ETC complex I activity and oxidative phosphorylation capacity.

### βII spectrin is localized in multiple mitochondrial sub-compartments

Given that IP–LC–MS/MS analysis revealed a large cohort of mitochondrial proteins, we next investigated whether βII spectrin is targeted to the mitochondria. We first assessed the possible presence of βII spectrin in the mitochondria by performing cell fractionation of NCMs and confirmed the presence of βII spectrin in the mitochondrial fractions, with no cross-contamination from the nuclear or the cytoplasmic fractions (Fig. 5a). We also performed immunofluorescence staining of NCMs and observed colocalization of βII spectrin and mitochondria (labeled with MitoTracker) (Fig. 5b). To determine which mitochondrial compartment is enriched with βII spectrin, we performed a protease protection assay of mitochondria in NCMs. Sizable amounts of mitochondrial βII spectrin loss accompanied the removal of the outer mitochondrial membrane (OMM) with a combination of trypsin and digitonin. However, considerable amounts of βII spectrin remained in mitochondria incubated with a combination of trypsin and digitonin (Fig. 5c, d), indicating that some βII spectrin is located inside the OMM. Additionally, βII spectrin was reduced in content but still present upon the removal of cytochrome c (Cyt C) (Fig. 5c, d), suggesting that βII spectrin is likely to reside in the intermembrane space (IMS) and matrix. Moreover, in situ immunogold labeling of thin sections of mouse heart mitochondria supported the localization of βII spectrin in the matrix, IMS, inner mitochondrial membrane (IMM) and OMM (Fig. 5e).

### βII spectrin interacts with mitochondrial complex I to mediate its assembly

To understand how βII spectrin regulates mitochondrial complex I activity, we first examined whether βII spectrin affects the expression of complex I subunits. We found that βII spectrin knockdown did not significantly affect the mRNA levels of the 44 subunits of complex I in NCMs (Supplementary Fig. 3a). Moreover, βII spectrin knockdown in NCMs did not significantly change the protein levels of the complex I subunits NDUFS1 and NDUFS3 (Supplementary Fig. 3b, c). These data suggest that βII spectrin knockdown does not significantly affect the expression of complex I subunits. However, IP–LC–MS/MS analysis revealed 31 complex I subunits that might bind to βII spectrin, suggesting that βII spectrin is likely to interact with complex I (Table 1). Indeed, our coimmunoprecipitation (co-IP) analysis confirmed that βII spectrin interacted endogenously with both NDUFS1 and NDUFS3 in either whole-cell lysates (WCLs) or purified mitochondrial fractions (Fig. 5f, g). Next, we investigated whether βII spectrin interacts with complex I to mediate its assembly. We found that both the amount of assembled complex I and the in-gel complex I activity were significantly decreased in βII spectrin cKO mice compared to control mice at 5 weeks post-tamoxifen treatment (Fig. 5h). Together, our data reveal that although βII spectrin does not affect the expression of complex I subunits, it interacts with complex I to regulate its assembly.

### βII spectrin controls mitochondrial complex I activity and mitochondrial function by stabilizing actin filaments

As actin filaments (F-actin), which are βII spectrin crosslinking proteins, have previously been reported to regulate mitochondrial respiratory function[21, 22], we next examined whether actin is involved in mitochondrial dysfunction caused by βII spectrin defects. We first assessed the possible presence of F-actin in the mitochondria by performing cell fractionation of NCMs and found that F-actin is certainly present within our mitochondrial preparations (Supplementary Fig. 4a). Moreover, in situ immunogold labeling of thin sections of mouse heart mitochondria showed that F-actin localized inside mitochondria (Supplementary Fig. 4b). We then performed co-IP analysis on either whole-cell lysates or purified mitochondrial fractions and found that F-actin physically interacted with both βII spectrin and NDUFS1 in NCMs (Fig. 6a, b). These data suggest that F-actin interacts with complex I in cardiomyocytes. F-actin is formed by the polymerization of globular actin monomers (G-actin) in a neat disposition that allows the filaments to be polarized[23]. The polymerization and depolymerization of actin filaments, as well as their organization into functional higher-order networks, are regulated by several actin-binding proteins[24, 25]. Although actin expression was unchanged in βII spectrin-knockdown NCMs, we observed significant decreases in the levels of F-actin in βII spectrin-knockdown NCMs via immunoblot and phalloidin staining (Fig. 6c–e), suggesting that βII spectrin is required for stabilization of F-actin. Therefore, we next treated NCMs with the F-actin stabilizer jasplakinolide to investigate whether restoring the stabilization of F-actin could reduce βII spectrin knockdown-induced mitochondrial dysfunction. As excessive polymerization of F-actin seems to trigger apoptosis[26, 27], we first investigated the effects of different concentrations of jasplakinolide on F-actin polymerization and cardiomyocyte apoptosis and found that 50 nM jasplakinolide dramatically upregulated F-actin levels without inducing apoptosis (Supplementary Fig. 5a–c). Treatment with jasplakinolide (50 nM) significantly increased the activity of complex I in βII spectrin-knockdown NCMs under normal as well as H/R conditions (Fig. 6f). Moreover, jasplakinolide (50 nM) treatment attenuated the βII spectrin knockdown-induced loss of mitochondrial membrane potential (Fig. 6g, h) and increase in mitochondrial ROS production (Fig. 6i, j) in NCMs under normal as well as H/R conditions. In addition, treatment with jasplakinolide (50 nM) reduced apoptosis in βII spectrin-knockdown NCMs under H/R conditions (Fig. 6k, l). In summary, these data demonstrate that βII spectrin regulates complex I activity, mitochondrial function and cardiomyocyte survival by stabilizing F-actin.

## Adenoviral intramyocardial βII spectrin saRNA transfer improves cardiomyocyte survival and mitochondrial function under I/R injury

βII spectrin is a large protein and is thus difficult to overexpress by synthesizing construct systems harboring exogenous DNA sequences. Previous studies have shown that saRNA can activate endogenous genes via an RNA-based promoter-targeting mechanism[28, 29]. To further demonstrate the role of βII spectrin in I/R injury, we restored βII spectrin expression by injecting adenoviruses coexpressing GFP and saRNA targeting selected promoter regions of βII spectrin into mouse hearts. Seven days after injection, these mice were subjected to I/R surgery or a sham operation (Supplementary Fig. 6a). We observed GFP-positive cardiomyocytes scattered around the injection site in the left ventricular myocardium at 7 days after injection (Supplementary Fig. 6b, c). Moreover, we identified two novel saRNAs (saRNA-54 and

saRNA-56) that successfully enhanced βII spectrin expression in cardiomyocytes (Supplementary Fig. 6d–f). We found that overexpression of βII spectrin mediated by both saRNA-54 and saRNA-56 markedly alleviated I/R-induced cardiac contractile dysfunction (Fig. 7a–c) and reduced the I/R-induced myocardial infarct size (Fig. 7d, e). In addition, overexpression of βII spectrin via both saRNA-54 and saRNA-56 in the heart resulted in resistance to I/R-induced myocardial apoptosis (Supplementary Fig. 6g–j) and necrosis, as evidenced by reductions in LDH levels and CK-MB release (Supplementary Fig. 6k, l). Notably, TEM analysis demonstrated that βII spectrin restoration via both saRNA-54 and saRNA-56 ameliorated I/R-induced mitochondrial morphological abnormalities (Fig. 7f–i). We further overexpressed βII spectrin in NCMs infected with adenoviruses expressing saRNA-54 and saRNA-56 (Supplementary Fig. 7a, b) and confirmed mitochondrial function via JC-1 staining and MitoSOX-based flow cytometry assays. We found that overexpression of βII spectrin via both saRNA-54 and saRNA-56 attenuated the H/R-induced mitochondrial membrane potential loss and increase in mitochondrial ROS production (Supplementary Fig. 7c–e); however, NDUFS1 knockdown blocked the protective role of saRNA-54 and saRNA-56 in these cells (Supplementary Fig. 7a–e). Collectively, our data demonstrate that restoration of βII spectrin expression via saRNA in the heart alleviates I/R-induced cardiac contractile dysfunction, cardiomyocyte death and mitochondrial damage.

# Discussion

Several novel observations are evident in the present study. First, we demonstrate for the first time that βII spectrin plays a critical role in maintaining cardiac contractile function under physiological conditions. Previous studies reported that systemic deletion of βII spectrin prevented cardiomyocyte differentiation and heart development[9, 10] and that conditional cardiac deletion of βII spectrin resulted in ventricular arrhythmia[12]. These results demonstrate that βIISP plays a significant role in cardiac development and cardiac electrophysiology. However, the role of βII spectrin in physiological cardiac contractile function has not been investigated. Based on an adult cardiac-specific βII spectrin deletion model, we found that βII spectrin deletion in the heart resulted in spontaneous development of contractile dysfunction, cardiac hypertrophy and fibrosis. Several spectrin isoforms, including αII, βII and βIV spectrin, have been reported to be expressed in the heart[8, 30]. In ventricular myocytes, αII and βII spectrin are found at the transverse-tubule and sarcoplasmic reticulum membranes[8], whereas βIV spectrin is located at the intercalated disc[30]. The three spectrins have been reported to play important roles in cardiovascular electrophysiology[12, 30, 31, 32]. However, cardiomyocyte-selective αII spectrin-deficient mice display cardiomyocyte hypertrophy and cardiac fibrosis[31]. A recent case report described patients with the homozygous stop mutation in the SPTBN4 gene (coding for βIV spectrin) presenting with hypertrophic cardiomyopathy[33]. This evidence and our results identify multiple roles of the spectrin-based cytoskeleton in the preservation of cardiac function.

Second, we provided the first evidence that ischemic downregulation of βII spectrin protein contributes to post-myocardial infarction pathologic remodeling. We found that βII spectrin protein was degraded into breakdown products by calpain in mouse hearts after I/R injury and that serum βII SBDPs levels were

significantly higher in AMI patients than in NOCAD patients. βII spectrin deletion in the adult heart worsens cardiomyocyte death and heart failure. In parallel, restoration of βII spectrin expression via saRNA in the heart reduces I/R injury. These results indicate that βII spectrin is a promising therapeutic target against I/R injury. Spectrin is a substrate for calpain, and calpain-mediated degradation of spectrin results in the formation of SBDPs, which could serve as potential biomarkers for the severity of neurologic insults[13, 14, 15]. Previous studies have revealed that αII and βII SBDPs can be detected in the cerebrospinal fluid[13, 15]. In this study, we observed that serum βII SBDPs are readily detectable. Moreover, we found that βII SBDPs levels were significantly higher in AMI patients than in NOCAD patients. saRNAs can activate endogenous genes by targeting selected sequences in gene promoters at both the transcriptional and epigenetic levels. Recent studies have shown that saRNAs not only provide new tools to study gene function and manipulate transcriptional activity but also have great promise for use in clinical therapy against various diseases[34, 35]. Herein, we identified two saRNAs that successfully enhance βII spectrin expression in cardiomyocytes and confirmed that both saRNAs alleviate I/R injury. Our findings identify a potential therapeutic use for saRNA in targeted βII spectrin gene activation.

Third, utilizing an unbiased approach, we identified βII spectrin as a critical regulator of mitochondrial homeostasis. Spectrins are cytoskeletal proteins essential for membrane stability and ion channel targeting[4, 5, 36]. There is currently very limited information on the roles of spectrins in organelle function. In this study, we report for the first time that βII spectrin is indispensable for preserving cardiomyocyte mitochondrial homeostasis. We found that βII spectrin localizes to mitochondria and interacts with mitochondrial complex I to mediate its assembly. Lack of βII spectrin provoked mitochondrial damage and respiratory dysfunction. Our findings demonstrate a role of βII spectrin as a mitochondrial cytoskeletal element that maintains mitochondrial function and cardiac function. A recent case report indicated that patients with a severe form of βIV spectrin deficiency present with mitochondrial dysfunction[33]. However, there is currently no information on the role of βII spectrin in regulating mitochondrial function. In the current study, we demonstrated that lack of βII spectrin provoked mitochondrial damage and respiratory dysfunction, suggesting that βII spectrin is a critical regulator of mitochondrial function. Moreover, we found that βII spectrin localized to mitochondria and existed in the matrix, IMS, IMM and OMM, suggesting that βII spectrin is a new cytoskeletal element that interacts with mitochondria. Importantly, we found that βII spectrin interacts with mitochondrial complex I and is indispensable for its assembly. Mitochondrial complex I is the initial and rate-limiting enzyme in the ETC. In the heart, mitochondrial complex I is highly susceptible to functional and structural destruction during I/R or heart failure, which contributes to myocardial energy insufficiency and cardiomyocyte death[37, 38]. In the present study, we found for the first time that defects in βII spectrin reduce mitochondrial complex I assembly, providing an explanation for the mechanisms by which mitochondrial complex I activity decreases during I/R or heart failure. Although our IP–LC–MS/MS analysis showed potential βII spectrin interactions with complexes II, III and IV in NCMs, we did not observe a significant change in complex II, III or IV activity in our βII spectrin-knockdown NCM models compared to the controls.

Finally, we demonstrated that βII spectrin regulates mitochondrial complex I activity, mitochondrial function and cardiomyocyte survival by crosslinking with F-actin to maintain F-actin stability. F-actin is the spectrin crosslinking protein and is formed by the polymerization of G-actin in a neat arrangement that allows the filaments to be polarized[23]. We and others[12] have observed that a lack of βII spectrin does not change actin protein levels in cardiomyocytes. However, in this study, we found that βII spectrin is required for the stabilization of F-actin in cardiomyocytes. This is consistent with the seeding role of erythrocyte spectrin in actin polymerization[39]. Furthermore, our data demonstrated that the F-actin stabilizer jasplakinolide alleviates βII spectrin deficiency-induced mitochondrial dysfunction and apoptosis, suggesting that βII spectrin regulates mitochondrial function by stabilizing F-actin. It has been established that F-actin localizes to mitochondria[40]. Most previous studies on the regulation of mitochondrial function by F-actin have focused on F-actin localization outside mitochondria to mediate mitochondrial dynamics[41, 42], trafficking and autophagy[43]. However, F-actin has been shown to localize inside mitochondria and contribute to mitochondrial DNA maintenance[44, 45]. As spectrin can crosslink with F-actin to form spectrin-actin arrays, this evidence and our results suggest that there may be a spectrin-actin cytoskeleton outside and inside mitochondria. In addition, we found that F-actin interacts with complex I in cardiomyocytes and that restoration of F-actin stability alleviates βII spectrin deficiency-induced complex I dysfunction. Importantly, a recent study showed that an ACTA1 (encoding skeletal alpha actin) mutation in a patient with nemaline myopathy caused mitochondrial complex I deficiency[46]. This evidence suggests that βII spectrin crosslinks with F-actin to maintain F-actin stability and therefore regulate mitochondrial complex I assembly and activity.

In summary, we have identified novel roles for βII spectrin in maintaining physiological cardiac function and attenuating post-ischemic pathological remodeling. βII spectrin is an essential mitochondrial cytoskeletal element for preserving mitochondrial homeostasis via interaction with mitochondrial complex I to mediate its assembly. Based on these findings, we propose that βII spectrin is a new therapeutic target for cardiac disorders such as I/R injury, myocardial infarction and heart failure.

# Methods

## Study population

In order to investigate whether βII spectrin could be degraded into breakdown products (βII spectrin breakdown products, βII SBDPs) in the heart after ischemic injury. We prospectively enrolled patients who were diagnosed with acute myocardial infarction (AMI) and Non-obstructive coronary artery disease (NOCAD) according to symptoms, electrocardiography, blood tests and coronary angiography in Xijing Hospital (Xi'an, China) from July 2020 to December 2020. In the present study, AMI was defined according to the fourth Universal Definition of Myocardial Infarction (2018). NOCAD was defined as stenosis <50% of the coronary artery diameter[47]. We enrolled all AMI patients and NOCAD patients consecutively except those who met the following exclusion criteria: (1) patients < 18 years old; (2) patients with hemodynamic instability; and (3) patients with new stroke or traumatic brain injury within 1

month. The study protocol was approved by the local institutional review board of Xijing Hospital and complied with the Declaration of Helsinki. Written informed consent was obtained from all patients.

The peripheral venous blood of AMI patients was collected 48 h after the onset of ischemia symptoms, and the peripheral venous blood of NOCAD patients was collected 48 h after admission. After the blood was clotted, the serum was collected and stored at −80°C until it was used for blinded determination of serum βII SBDPs levels. The serum levels of βII SBDPs were detected with a standard enzyme-linked immunosorbent assay (ELISA) kit (Biorbyt, orb756702).

## Animals

All animal experimental protocols were performed strictly in accordance with the National Institutes of Health Guidelines on the Use of Laboratory Animals (NIH publication No. 85-23, revised 2011) and were approved by the Animal Care and Use Committee of the Air Force Medical University. Adult (10- to 12-week-old) male and neonatal (1- to 3-day-old) C57BL/6J mice were purchased from the Laboratory Animal Center of the Air Force Medical University. All animals were maintained under a 12-h:12-h light:dark cycle in constant-temperature rooms. Chow food and water were available ad libitum.

βII spectrin$^{flox/flox}$ mice were purchased from the Jackson Laboratory (Stock No: 020288, USA). The loxP sites were inserted into introns flanking exon 3 of the mouse SPTBN1 locus via homologous recombination. αMHC-CreERT2-βII spectrin$^{flox/flox}$ mice were obtained by crossing βII spectrin$^{flox/flox}$ mice and tamoxifen-inducible αMHC-CreERT2 transgenic mice. βII spectrin$^{flox/flox}$ Cre− littermates and αMHC-Cre+ littermates were used as control mice. Both αMHC-CreERT2-βII spectrin$^{flox/flox}$ mice and control mice (aged from 10-12 weeks) were treated with the same tamoxifen regimen for a total of 7 consecutive days. For Cre characterization work, there was a 7-day waiting period before the subsequent animal experiment.

The following primers were used for genotyping:

| Genotype | Forward | Reverse |
|---|---|---|
| βII spectrin $^{flox/flox}$: | 5’-GTAGCCTCCTTTCTGGGATG-3’ | 5’-TAGAGCCCCTTCCATGGTCT-3’ |
| αMHC-Cre: | 5’-ATACCGGAGATCATGCAAGC-3’ | 5’-AGGTGGACC TGATCATGGAG-3’ |

## Adenovirus construction and gene delivery *in vivo*

For gene-silencing assays, recombinant adenoviral vectors carrying SPTBN1-specific shRNA (Ad-sh-SPTBN1) and scramble control vectors (Ad-scramble) were constructed by GeneChem Co., Ltd. (Shanghai, China). For overexpression, recombinant adenoviral vectors carrying saRNAs targeting the promoter region (-41 to -21 bp and -567 to -547 bp upstream of the transcription start site) of the SPTBN1

gene (Ad-saRNA-54 or Ad-saRNA-56) and scramble vectors (Ad-control) were designed and synthesized by GeneChem Co., Ltd. (Shanghai, China).

The adenoviral vectors were delivered into the heart via intramyocardial injection as previously described[48]. Briefly, mice were anesthetized using 2.5% isoflurane during the surgical procedure. After a left thoracic incision to expose the heart, the adenoviruses were resuspended in PBS at $2.5\times10^{11}$ pfu/ml and intramyocardially injected at 3 different sites (10 μl per site) from the apex of the left ventricle free wall to the aortic root using a 30-gauge needle. Finally, the chest was carefully closed. At day 7 after adenovirus injection, the transduction efficiency of the adenovirus was examined by analysis of protein expression and the presence of GFP in the heart. Then, the mice underwent myocardial sham or I/R operation.

All sequences are listed as follows:

| shRNA/saRNA | Sense | Antisense |
|---|---|---|
| Ad-scramble: | 5’-TTCTCCGAACGTGTCACGT-3’ | 5’-ACGTGACACGTTCGGAGAA-3’ |
| Ad-sh-SPTBN1: | 5’-GCGGCTCTTTGATGCAAAT-3’ | 5’-ATTTGCATCAAAGAGCCGC-3’ |
| Ad-control: | 5'-CAGTCGCGTTTGCGACTGG-3' | 5’- CCAGTCGCAAACGCGACTG-3’ |
| Ad-saRNA-54: | 5’-AGTTCTTAAGACCAGTAATCC-3’, | 5’-GGATTACTGGTCTTAAGAACT-3’ |
| Ad-saRNA-56: | 5’-ACTTTGTATACACACCTGTGC-3’ | 5’-GCACAGGTGTGTATACAAAGT -3’ |
| siCtrl | 5’-UUCUCCGAACGUGUCACGUTT-3’ | 5’-ACGUGACACGUUCGGAGAATT-3’ |
| siNDUFS1 | 5’-GCAUGCAAAUCCCUCGAUUTT-3’ | 5’-AAUCGAGGGAUUUGCAUGCTT-3’ |

## Myocardial ischemia/reperfusion (I/R) model

A mouse model of myocardial I/R injury was established as we previously described[49]. In brief, all mice were anesthetized with 1-2% isoflurane throughout the procedure. A left thoracotomy was performed to exteriorize the heart, and a silk suture (6–0) slipknot was reversibly tied around the left anterior descending (LAD) coronary artery. After 30 minutes of ischemia, reperfusion was induced by releasing the slipknot. Sham mice underwent the same surgical procedures without LAD coronary artery ligation. Mice were sacrificed after 3 h (to detect caspase-3 activation), 24 h (to detect cardiac function, the concentrations of lactate dehydrogenase (LDH) and creatine kinase-MB (CK-MB), infarct size and cardiac apoptosis) and 28 days (to measure long-term cardiac function and cardiac fibrosis) of reperfusion.

## LDH and CK-MB measurement

To determine the concentrations of serum LDH and CK-MB, blood was drawn from the carotid artery after 24 h of reperfusion. The serum was collected after centrifugation at 1000 rpm for 10 minutes at 4°C and stored at -80°C. The concentrations of LDH and CK-MB were measured using an LDH ELISA kit (LSBio, F54173) and a CK-MB ELISA kit (LSBio, F20753), respectively.

### Echocardiography

M-mode images of mice under 1-2% isoflurane anesthesia were obtained via an echocardiographic imaging system (Vevo 2100, VisualSonics, Canada) as previously described[50]. Two-dimensional echocardiographic views of the mid-ventricular short axis and long axis were collected between the two papillary muscles. The LVEF, LVFS, LVESD and LVEDD were measured as we have previously described[51].

### Evaluation of cardiomyocyte apoptosis

Apoptosis was detected *in vivo* and *in vitro* using a TUNEL kit (Beyotime, C1090) according to the manufacturer's instructions. The apoptosis level was calculated by dividing the number of TUNEL-positive nuclei by the total number of 4',6-diamidino-2-phenylindole (DAPI)-positive nuclei. Apoptosis was evaluated in at least 5 randomly selected fields in each heart section or in cardiomyocytes. The *in vitro* apoptosis rate was also determined by flow cytometry analysis using an Annexin V-FITC/propidium iodide (PI) apoptosis detection kit (Beyotime, C1062S) according to the manufacturer's instructions.

### Evans blue/triphenyltetrazolium chloride (TTC) double staining

To evaluate infarct size, Evans/TTC double staining was performed at the end of 24 h of reperfusion as previously described[52]. Mice were placed under 1-2% isoflurane anesthesia, and the LAD coronary artery was retied with a suture in the original position. Two percent Evans blue dye (Sigma, E2129) in PBS was injected into the brachiocephalic artery to visualize nonischemic tissue (blue area) and ischemic tissue (area at risk, AAR). After being excised, the heart was frozen on a block of dry ice for 15 minutes and cut horizontally into five 1-mm-thick slices. Then, the slices were incubated with 1% TTC (Sigma, T8877) in PBS at 37°C for 15 minutes to visualize the infarct size (IS, white area) and viable myocardial tissue (red area). The red plus white area indicates the AAR. ImageJ software was used to measure the AAR and infarct area from the third section, and the values obtained were averaged.

### Masson's trichrome and wheat germ agglutinin staining

In brief, hearts were collected, fixed in 10% neutralized formalin, embedded in paraffin and sectioned into 5-μm-thick slices. The sections were stained with Masson's trichrome (Sigma, HT15) and FITC-conjugated wheat germ agglutinin antibodies according to the manufacturer's protocol. Images were obtained with a microscope (Nikon, Japan). Fibrosis amount was determined as the ratio of the fibrotic area to the left ventricle area.

### Isolation, culture and adenoviral infection of cardiomyocytes

Neonatal mouse cardiomyocytes (NCMs) were isolated from 1- to 3-day-old neonatal C57/BL6J mice as previously described[53]. Briefly, the hearts from suckling mice were excised and fully washed with PBS under aseptic conditions. The ventricular tissues were minced with sterile scissors and digested with buffer containing 1 mg/mL collagenase type II (Gibco, 17101015) for 3 min at 37°C. The digestion was repeated until the digestion fluid became clear (approximately 4–6 times). Cardiomyocytes were collected by differential plating and cultured in Dulbecco's modified Eagle's medium (DMEM) containing 20% fetal bovine serum (FBS) and 1% penicillin–streptomycin. After another 48 h to completely plate, the NCMs were subjected to various treatments, including adenoviral infection and H/R.

Cardiomyocytes were infected with recombinant adenoviruses for 12 h at a multiplicity of infection (MOI) of 50. The medium containing virus was then replaced with fresh medium, and the cells were cultured for another 48 h. The efficiency of gene overexpression and knockdown was detected by western blot analysis.

### Hypoxia/reoxygenation (H/R) *in vitro* and drug treatment

To mimic I/R injury *in vivo*, *in vitro* H/R models were established in NCMs. Briefly, NCMs were subjected to 4 h of hypoxia and 2 h of reoxygenation. To induce hypoxia, NCMs were cultured in a hypoxia chamber with 95% $N_2$ and 5% $CO_2$ at 37°C in serum-free and glucose-free medium. For reoxygenation, the NCMs were cultured in culture medium (DMEM 90%, FBS 10%, 1% penicillin–streptomycin) for 2 h in an incubator with 21% $O_2$ and 5% $CO_2$.

To inhibit calpain activity, the calpain inhibitor T2470 (Topscience, 88191-84-8, 100 μM) was added to cultured cardiomyocytes 30 min before H/R treatment. To promote actin polymerization, cardiomyocytes were treated with jasplakinolide (Sigma, J4580, 50 nM) for 2 h before H/R treatment.

### Cell viability

Cell viability was detected with CCK-8 assays (Topscience, C0005). Briefly, after H/R treatment, NCMs were cultured in fresh medium containing 10% CCK-8 reagent for 2 h. The absorbance at 450 nm was detected to indicate cell viability.

### Isolation of mitochondria

Mitochondria were isolated from NCMs using a Cell Mitochondria Isolation Kit (Beyotime, C3601) according to the manufacturer's protocols. Briefly, $1.0\times10^7$ cardiomyocytes were homogenized in ice-cold isolation buffer and centrifuged at 1000 ×g for 10 minutes at 4°C. After the supernatant was centrifuged at 5000 ×g and 4°C for 10 minutes, the pellet was washed twice with isolation buffer by centrifugation at 3000 ×g for 10 minutes at 4°C. Mitochondria-enriched fractions were resuspended in mitochondrial storage buffer and stored at -80°C until further analyses, including analysis of ETC complex activity and western blotting. To perform a protease protection assay, mitochondria were incubated in the presence of different concentrations of digitonin (Topscience, T2721) for 30 minutes at room temperature. Then, the

mitochondria were centrifuged at 3000 ×g for 10 minutes at 4°C, and the pellet was boiled in 1× SDS–PAGE sample loading buffer at 95°C for 5 minutes for western blot analysis.

### Mitochondrial ETC complex activity

Mitochondrial ETC complex activity was detected using various mitochondrial complex activity assay kits according to the manufacturers' instructions. Mitochondrial complex I activity was measured by following the oxidation of NADH to NAD+ as an absorbance decrease at OD=450 nm using a Mitochondrial Complex I Activity Assay Kit (Abcam, ab109721). Mitochondrial complex II activity was calculated by measuring the rate of 2,6-dichlorophenol decrease as an absorbance decrease at OD=605 nm using a Mitochondrial Complex II Activity Assay Kit (Solarbio, BC3230). Mitochondrial complex III activity was calculated by measuring the rate of reduced cytochrome C increase as an absorbance increase at 550 nm using a Mitochondrial Complex III Activity Assay Kit (Solarbio, BC3245). Mitochondrial complex IV activity was determined colorimetrically by assessing the oxidation of reduced cytochrome C as an absorbance decrease at 550 nm using a Mitochondrial Complex IV Activity Assay Kit (Abcam, ab109911).

### Mitochondrial ROS and membrane potential measurements

Mitochondrial ROS production in NCMs was measured with MitoSOX Red (Thermo Fisher Scientific, M36008). Briefly, NCMs were harvested and loaded with 5 μM MitoSOX Red for 10 minutes at 37°C. After three washes with PBS, fluorescence was detected with a BD FACS Aria II flow cytometer.

Mitochondrial membrane potential was assessed with a Mitochondrial Membrane Potential JC-1 Kit (Beyotime, C2006). In brief, cardiomyocytes were harvested and loaded with JC-1 working buffer for 20 minutes at 37°C. After the cells were washed three times with PBS, fluorescence was measured via flow cytometry. When the mitochondrial membrane potential was high, JC-1 aggregated in the mitochondrial matrix and emitted red fluorescence. When the mitochondrial membrane potential was low, JC-1 could not aggregate in the mitochondrial matrix and existed as a monomer, exhibiting green fluorescence. The ratio of red to green fluorescence was used to measure the ratio of mitochondrial depolarization.

### ATP measurements

The cellular ATP content was measured with an ATP bioluminescence kit (Beyotime, S0027) following the protocols provided by the manufacturer. Briefly, NCMs were collected and lysed in lysis buffer. After centrifugation at 12000 ×g and 4°C for 10 minutes, the supernatant was taken for subsequent determination. Then, 100 μL of reaction buffer was added to 96-well plates at room temperature for 3-5 minutes to allow all background ATP to be consumed. Ten microliters of standard ATP solution or sample lysate was added to each well. Measurements were performed with a luminometer (BioTek Epoch, USA).

### Seahorse analysis

The mitochondrial OCR was recorded with an XF24 Extracellular Flux Analyzer (Agilent Seahorse Bioscience, USA). Briefly, NCMs were seeded into XF24 Seahorse plates at a density of 160,000 cells/well and infected with adenoviruses for 48 h. After the NCMs were subjected to normoxia or H/R, the OCR was measured according to the manufacturer's protocol. The optimal concentrations of the inhibitors were as follows: oligomycin, 0.6 μM; trifluoromethoxy carbonyl cyanide phenylhydrazone (FCCP), 0.75 μM; antimycin A, 2 μM; and rotenone, 1 μM. Basal respiration, maximal respiration, ATP production and spare respiration capacity were calculated using XF Cell Mito Stress Test Generator software (Agilent Seahorse Bioscience, USA).

### Analysis of mitochondrial complexes

Mitochondria were isolated as described above. Every 200 μg of mitochondria was resuspended in 40 μl of extraction buffer (50 mM sodium chloride, 50 mM imidazole, 2 mM 6-aminohexanoic acid, 1 mM EDTA, pH 7.0) and solubilized with digitonin at a final concentration of 6 g/g mitochondrial proteins on ice for 20 minutes. Each sample was centrifuged at 17000 ×g and 4°C for 10 minutes. Then, 100 μg of proteins per sample was loaded and separated on a NativePAGE™ 3%-12% gel (ThermoFisher Scientific, #BN1001BOX). For blue native PAGE (BN-PAGE), the gel was scanned and quantified using ImageStudio software. For visualization of the enzymatic activity of complex I, in-gel assays (IGAs) were performed after clear native PAGE (CN-PAGE). The gel was soaked in 20 mL of 10 mM Tris/HCl pH 7.4 containing NTB (50 mg) and 200 mL of 10 mg/mL NADH.

### Quantitative PCR

Total RNA was extracted from heart tissues or cardiomyocytes via TRIzol reagent (Thermo Fisher Scientific, 15596026). The RNA was reverse-transcribed into cDNA and amplified using a PrimeScript RT Reagent Kit with gDNA Eraser (Takara, Japan, RR047A). Quantitative real-time PCR was performed via SYBR Green PCR Master Mix (Takara, Japan, RR820A) on an Applied Biosystems ABI Prism machine. The thermal cycling conditions were as follows: denaturation at 95°C for 30 s followed by 40 cycles of 5 s at 95°C and 30 s at 60°C. The primers were purchased from Tsingke Biotechnology (Shanghai, China). Gene expression was calculated using the standard comparative CT method and normalized to the expression of β-actin. The primer sequences were as follows:

| Gene | Forward | Reverse |
|---|---|---|
| βII spectrin | 5'-CCAGACTGCTATCGCCTCAG-3' | 5'-AGCTCATTCCAGCCAGTGTC-3' |
| β-actin | 5'-AACAGTCCGCCTAGAAGCAC-3' | 5'-CGTTGACATCCGTAAAGACC-3' |

### Western blot analysis

Total proteins were extracted from cultured cardiomyocytes or heart tissues with RIPA lysis buffer (25 mM Tris-HCl pH 7.6, 150 mM NaCl, 1% NP-40, 1% sodium deoxycholate and 0.1% SDS; Thermo Fisher Scientific, 89901) supplemented with a protease and phosphatase inhibitor cocktail (CST, 5872). The protein concentrations were quantified using a bicinchoninic acid (BCA) protein assay kit (Thermo Fisher Scientific, 23225). A total of 20-40 μg of protein per sample was separated via gel electrophoresis and transferred onto polyvinylidene fluoride (PVDF) membranes. After blocking with 5% fat-free milk for 1 h at room temperature, the membranes were incubated with primary antibodies at 4°C overnight. After incubation with a secondary anti-mouse antibody (Abbkine, A21010, 1/10,000) or anti-rabbit antibody (Abbkine, A21020, 1/10,000) at room temperature for 1 h, the membranes were visualized with enhanced chemiluminescence (ECL) substrate (Thermo Fisher Scientific, 34096) and scanned with a ChemiDoc XRS system (Bio-Rad Laboratory, USA). Densitometric analyses of the immunoblots were performed using ImageJ software (NIH, USA).

The following primary antibodies were used in this study: anti-SPTBN1 (Abcam, ab72239), anti-cleaved caspase-3 (CST, 9661), anti-Caspase-3 (CST, 9662), anti-Ndufs1 (Proteintech, 12444-1-AP), anti-Ndufs3 (Abclonal, A8013), anti-VDAC1 (CST, 4866), anti-β-actin (CST, 3700), anti-F-actin (Abcam, ab130935), anti-HSP90 (CST, 4877), anti-TOMM20 (Proteintech, 11802-1-AP), anti-Cytochrome C (Proteintech, 66264-1-Ig), anti-citrate synthase (Proteintech, 16131-1-AP), and anti-GAPDH (CST, 5174).

### Coimmunoprecipitation

NCMs were washed with ice-cold PBS three times and lysed with IP lysis buffer (25 mM Tris-HCl pH 7.4, 150 mM NaCl, 1% NP-40, 1 mM EDTA and 5% glycerol; Thermo Fisher Scientific, 87787) supplemented with a protease and phosphatase inhibitor cocktail (CST, 5872). The lysates were incubated with 1 μg of antibodies for immunoprecipitation at 4°C overnight. Protein A/G magnetic beads were added for 3 h at 4°C. After the beads were washed with IP lysis buffer three times, the protein samples containing dithiothreitol were heated and separated by electrophoresis. After transfer to PVDF membranes, the proteins were immunoblotted with anti-βII spectrin, anti-NDUFS1, and anti-NDUFS antibodies. Forty microliters of cell lysates were saved for use as positive controls and loading controls in immunodetection.

### LC–MS/MS analysis

Liquid chromatography tandem mass spectrometry (LC–MS/MS) experiments were performed at Bioprofile Co., Ltd. (Shanghai, China) on a Q Exactive HF-X mass spectrometer coupled to an Easy nLC1200 system (Thermo Scientific). Briefly, the in-gel samples were denatured and alkylated. Then, precooled acetone was added to precipitate the proteins. The protein precipitates were resolved and digested with trypsin (Promega) at a protein:enzyme ratio of 50:1 at 37°C overnight. The peptides were collected by centrifugation at 16 000 ×g and 20°C for 15 min. The peptides were desalted with C18 StageTips for further LC–MS analysis. The peptides were first loaded onto a trap column in buffer A (0.1% formic acid in water). Reverse-phase high-performance liquid chromatography (RP–HPLC) separation was performed using a self-packed column at a flow rate of 300 nL/min. Mass spectrometry

(MS) data were acquired using a data-dependent top 20 method with dynamic selection of the most abundant precursor ions from the survey scan (350–1800 m/z) for higher-energy collisional dissociation (HCD) fragmentation. The full MS scans were acquired at a resolution of 60,000 at m/z 200, while 15,000 at m/z 200 was used for the MS/MS scan. The MS data were analyzed using MaxQuant software version 1.6.1.0. The MS data were searched against the UniProtKB mouse database (www.UniProt.org).

### RNA sequencing (RNA-seq) analysis

NCMs were infected with adenoviruses for 48 h. Total RNA was extracted for RNA-seq analysis by CapitalBio Co., Ltd. For mRNA library construction and deep sequencing, RNA samples were prepared using a TruSeq RNA Sample Preparation Kit according to the manufacturer's protocol. In brief, purified poly-A-containing mRNA molecules were obtained from 3 μg of total RNA using poly-T oligo-attached magnetic beads. The cleaved RNA fragments were reverse-transcribed into first-strand cDNA using random hexamers, after which second-strand cDNA synthesis was performed using DNA Polymerase I and RNase H. The cDNA fragments were purified, end-blunted, 'A'-tailed, and adaptor ligated. PCR was used to selectively enrich the DNA fragments with adapter molecules on both ends and to amplify the amount of DNA in the library. The number of PCR cycles was minimized to avoid skewing the representation of the library. The library was qualified with an Agilent 2100 bioanalyzer and quantified via Qubit and qPCR. The produced library was sequenced on an Illumina NovaSeq 6000 platform. Differentially expressed genes (DEGs) were defined as genes with a |log2(fold change)| > 1 and an adjusted p value < 0.05.

### Immunofluorescence staining

For immunofluorescence analyses, NCMs were fixed with 4% paraformaldehyde for 10 minutes, permeabilized in 0.3% Triton X-100 for 10 minutes, and blocked with 5% bovine serum albumin (BSA) in PBS for 1 h. The cells were incubated with an anti-βII spectrin antibody (Abcam, ab72239) overnight at 4°C. After washing with PBS three times, the cells were incubated with a goat anti-rabbit IgG (H+L) secondary antibody conjugated with Alexa Fluor 488 (Thermo Fisher Scientific, A-11008) for 1 h at room temperature. The nuclei were stained with DAPI (Beyotime, C1005). Images were obtained with a confocal laser scanning microscope (Nikon, Japan).

To label mitochondria, live cardiomyocytes were stained with the MitoTracker™ Red CMXRos probe (Thermo Fisher Scientific, M7512) using a working concentration of 150 nM at 37°C for 20 min. The cells were fixed and permeabilized as described above for subsequent manipulations. To view F-actin organization, NCMs were incubated with a CoraLite® 594-conjugated phalloidin antibody (Proteintech, PF00003) for 40 minutes after fixation and permeabilization as described above.

### Transmission electron microscopy

The mouse hearts were perfused, and the left ventricular walls were cut perpendicularly to the long axis into 1-2 mm wide rings. These rings were fixed with 2.5% glutaraldehyde in 0.1 mol/l phosphate buffer

(pH 7.4, 4°C) for 24 h and postfixed with 1% osmium tetroxide in 0.1 mol/l sodium cacodylate buffer (pH 7.4, 4°C) for 1 h. Then, the rings were dehydrated, embedded in resin and cut into 80 nm-thick sections. All images were captured with a transmission electron microscope (JEM-1230, JEOL Ltd., Japan) at 80 kV. Mitochondrial images were obtained at 28,000 and 98,000 magnifications and analyzed using ImageJ software.

### Immunoelectron microscopy

The mouse left ventricles were cut into rings as described above. The rings were fixed with 3.0% glutaraldehyde, dehydrated using a graded ethanol immersion series, embedded in resin and cut into 80 nm-thick sections. The sections were blocked with 1% BSA for 20 minutes at room temperature and incubated with an anti-βII spectrin antibody (Abcam, ab72239) for 20 hours. After being rinsed three times with PBS, the sections were again incubated with 1% BSA and subsequently incubated with anti-rabbit colloidal gold (Bioss, bs-0295G-Gold) for 2 h at room temperature. Uranium acetate and lead citrate were added. After being rinsed three times with PBS, the sections were viewed with a transmission electron microscope (JEM-1230, JEOL Ltd., Japan) at 80 kV. Mitochondrial images were obtained at 80,000× magnification.

### Statistical analysis

Continuous variables are presented as the mean ± standard deviation. The normality of the data distribution was examined using a Shapiro–Wilk normality test. Two-tailed Student's t test and Mann–Whitney U test were conducted to compare differences between two groups. For multiple-group comparisons with one independent variable, one-way ANOVA followed by Tukey's multiple comparisons test was conducted. Differences at different time points or concentrations were evaluated using one-way ANOVA followed by Dunnett's multiple comparisons test. Log-rank Mantel-Cox testing was performed for survival analysis. $P$ values <0.05 were considered to indicate statistical significance. The data were analyzed using GraphPad Prism software 8.3.0. (Graph Pad, Inc., USA) and SPSS Statistics, version 25 (IBM Corp., Armonk, 281 N.Y., USA).

# Declarations


### Acknowledgments

We thank Shanghai Bioprofile Technology Company Ltd. for technological assistance in IP–LC–MS/MS analysis. This work was financially supported by the Program for National Science Funds of China (Grant Nos. 81730011, 82070867, 81600683, 81970721 and 81927805), the National Key R&D Program of China (Grant No. 2018YFA0107400), and the Program for Changjiang Scholars and Innovative Research Team in University (Grant No. PCSIRT-14R08).


### Author contributions

R.J.Y., B.J.R., R.T.W., X.M.Z., P.P.XP, C.Y.L., Y.Y.Z., X.Q.C., S.Z., H.S.Z., F.Y.Z., T.Y., T.T.Q., W.J.Y.,F.Y.Z. and G.Y.H. performed experiments, analyzed data and reviewed the manuscript. S.W. and L.T. designed experiments, analyzed data, and wrote the manuscript. L.T. is the guarantor of this study. All authors approved the final version of the manuscript.

### Competing interests

The authors declare no competing interests.

# References


1. Hohmann T, Dehghani F. The Cytoskeleton-A Complex Interacting Meshwork. Cells **8**, (2019).
2. Fletcher DA, Mullins RD. Cell mechanics and the cytoskeleton. Nature **463**, 485–492 (2010).
3. Winkelmann JC, Forget BG. Erythroid and nonerythroid spectrins. Blood **81**, 3173–3185 (1993).
4. Patel-Hett S, *et al.* The spectrin-based membrane skeleton stabilizes mouse megakaryocyte membrane systems and is essential for proplatelet and platelet formation. Blood **118**, 1641–1652 (2011).
5. Bennett V, Lorenzo DN. Spectrin- and ankyrin-based membrane domains and the evolution of vertebrates. Current topics in membranes **72**, 1–37 (2013).
6. Bennett V, Lorenzo DN. An Adaptable Spectrin/Ankyrin-Based Mechanism for Long-Range Organization of Plasma Membranes in Vertebrate Tissues. Current topics in membranes **77**, 143–184 (2016).
7. Bennett V, Baines AJ. Spectrin and ankyrin-based pathways: metazoan inventions for integrating cells into tissues. Physiological reviews **81**, 1353–1392 (2001).
8. Baines AJ, Pinder JC. The spectrin-associated cytoskeleton in mammalian heart. Frontiers in bioscience: a journal and virtual library **10**, 3020–3033 (2005).
9. Tang Y, Katuri V, Dillner A, Mishra B, Deng CX, Mishra L. Disruption of transforming growth factor-beta signaling in ELF beta-spectrin-deficient mice. Science (New York, NY) **299**, 574–577 (2003).
10. Lim JA, *et al.* Loss of β2-spectrin prevents cardiomyocyte differentiation and heart development. Cardiovascular research **101**, 39–47 (2014).
11. Smith SA, *et al.* Dysfunction of the β2-spectrin-based pathway in human heart failure. American journal of physiology Heart and circulatory physiology **310**, H1583-1591 (2016).
12. Smith SA, *et al.* Dysfunction in the βII spectrin-dependent cytoskeleton underlies human arrhythmia. Circulation **131**, 695–708 (2015).
13. Pineda JA, *et al.* Clinical significance of alphaII-spectrin breakdown products in cerebrospinal fluid after severe traumatic brain injury. Journal of neurotrauma **24**, 354–366 (2007).
14. Schober ME, *et al.* Alpha II Spectrin breakdown products in immature Sprague Dawley rat hippocampus and cortex after traumatic brain injury. Brain research **1574**, 105–112 (2014).

15. Kobeissy FH, *et al.* Degradation of βII-Spectrin Protein by Calpain-2 and Caspase-3 Under Neurotoxic and Traumatic Brain Injury Conditions. Molecular neurobiology **52**, 696–709 (2015).
16. Andersson HB, *et al.* Long-term survival and causes of death in patients with ST-elevation acute coronary syndrome without obstructive coronary artery disease. European heart journal **39**, 102–110 (2017).
17. Chen M, He H, Zhan S, Krajewski S, Reed JC, Gottlieb RA. Bid is cleaved by calpain to an active fragment in vitro and during myocardial ischemia/reperfusion. The Journal of biological chemistry **276**, 30724–30728 (2001).
18. French JP, *et al.* Ischemia-reperfusion-induced calpain activation and SERCA2a degradation are attenuated by exercise training and calpain inhibition. American journal of physiology Heart and circulatory physiology **290**, H128-136 (2006).
19. Hernando V, Inserte J, Sartório CL, Parra VM, Poncelas-Nozal M, Garcia-Dorado D. Calpain translocation and activation as pharmacological targets during myocardial ischemia/reperfusion. Journal of molecular and cellular cardiology **49**, 271–279 (2010).
20. Czogalla A, Sikorski AF. Spectrin and calpain: a 'target' and a 'sniper' in the pathology of neuronal cells. Cellular and molecular life sciences: CMLS **62**, 1913–1924 (2005).
21. Lin S, *et al.* Fascin Controls Metastatic Colonization and Mitochondrial Oxidative Phosphorylation by Remodeling Mitochondrial Actin Filaments. Cell reports **28**, 2824–2836.e2828 (2019).
22. Takahashi K, Miura Y, Ohsawa I, Shirasawa T, Takahashi M. In vitro rejuvenation of brain mitochondria by the inhibition of actin polymerization. Scientific reports **8**, 15585 (2018).
23. Dominguez R, Holmes KC. Actin structure and function. Annual review of biophysics **40**, 169–186 (2011).
24. Lappalainen P. Actin-binding proteins: the long road to understanding the dynamic landscape of cellular actin networks. Molecular biology of the cell **27**, 2519–2522 (2016).
25. Merino F, Pospich S, Raunser S. Towards a structural understanding of the remodeling of the actin cytoskeleton. Seminars in cell & developmental biology **102**, 51–64 (2020).
26. Posey SC, Bierer BE. Actin stabilization by jasplakinolide enhances apoptosis induced by cytokine deprivation. The Journal of biological chemistry **274**, 4259–4265 (1999).
27. Odaka C, Sanders ML, Crews P. Jasplakinolide induces apoptosis in various transformed cell lines by a caspase-3-like protease-dependent pathway. Clinical and diagnostic laboratory immunology **7**, 947–952 (2000).
28. Li LC, *et al.* Small dsRNAs induce transcriptional activation in human cells. Proceedings of the National Academy of Sciences of the United States of America **103**, 17337–17342 (2006).
29. Janowski BA, Younger ST, Hardy DB, Ram R, Huffman KE, Corey DR. Activating gene expression in mammalian cells with promoter-targeted duplex RNAs. Nature chemical biology **3**, 166–173 (2007).
30. Hund TJ, *et al.* A β(IV)-spectrin/CaMKII signaling complex is essential for membrane excitability in mice. The Journal of clinical investigation **120**, 3508–3519 (2010).

31. Lubbers ER, *et al.* Defining new mechanistic roles for αII spectrin in cardiac function. **294**, 9576–9591 (2019).
32. Hund TJ, *et al.* β(IV)-Spectrin regulates TREK-1 membrane targeting in the heart. Cardiovascular research **102**, 166–175 (2014).
33. Belkheir AM, *et al.* Severe Form of ßIV-Spectrin Deficiency With Mitochondrial Dysfunction and Cardiomyopathy-A Case Report. Frontiers in neurology **12**, 643805 (2021).
34. Zhou LY, He ZY, Xu T, Wei YQ. Current Advances in Small Activating RNAs for Gene Therapy: Principles, Applications and Challenges. Current gene therapy **18**, 134–142 (2018).
35. Ghanbarian H, Aghamiri S. Small Activating RNAs: Towards the Development of New Therapeutic Agents and Clinical Treatments. **10**, (2021).
36. Nassal D, *et al.* Regulation of Cardiac Conduction and Arrhythmias by Ankyrin/Spectrin-Based Macromolecular Complexes. Journal of cardiovascular development and disease **8**, (2021).
37. Paradies G, Petrosillo G, Pistolese M, Di Venosa N, Federici A, Ruggiero FM. Decrease in mitochondrial complex I activity in ischemic/reperfused rat heart: involvement of reactive oxygen species and cardiolipin. Circulation research **94**, 53–59 (2004).
38. Ide T, *et al.* Mitochondrial electron transport complex I is a potential source of oxygen free radicals in the failing myocardium. Circulation research **85**, 357–363 (1999).
39. Sato SB, Yanagida M, Maruyama K, Ohnishi S. Seeding role of spectrin in polymerization of skeletal muscle actin. Biochimica et biophysica acta **578**, 436–444 (1979).
40. Illescas M, Peñas A, Arenas J, Martín MA, Ugalde C. Regulation of Mitochondrial Function by the Actin Cytoskeleton. Frontiers in cell and developmental biology **9**, 795838 (2021).
41. Moore AS, Wong YC, Simpson CL, Holzbaur EL. Dynamic actin cycling through mitochondrial subpopulations locally regulates the fission-fusion balance within mitochondrial networks. Nature communications **7**, 12886 (2016).
42. Tilokani L, Nagashima S, Paupe V, Prudent J. Mitochondrial dynamics: overview of molecular mechanisms. Essays in biochemistry **62**, 341–360 (2018).
43. Kast DJ, Dominguez R. The Cytoskeleton-Autophagy Connection. Current biology: CB **27**, R318-r326 (2017).
44. Lo YS, *et al.* Actin in mung bean mitochondria and implications for its function. The Plant cell **23**, 3727–3744 (2011).
45. Reyes A, *et al.* Actin and myosin contribute to mammalian mitochondrial DNA maintenance. Nucleic acids research **39**, 5098–5108 (2011).
46. Pula S, *et al.* A novel de novo ACTA1 variant in a patient with nemaline myopathy and mitochondrial Complex I deficiency. Neuromuscular disorders: NMD **30**, 159–164 (2020).
47. Andersson H, *et al.* Long-term survival and causes of death in patients with ST-elevation acute coronary syndrome without obstructive coronary artery disease. European heart journal **39**, 102–110 (2018).

48. Gao C, *et al.* TXNIP/Redd1 signalling and excessive autophagy: a novel mechanism of myocardial ischaemia/reperfusion injury in mice. Cardiovascular research **116**, 645–657 (2020).
49. Gao E, *et al.* A novel and efficient model of coronary artery ligation and myocardial infarction in the mouse. Circulation research **107**, 1445–1453 (2010).
50. Xia Y, *et al.* Adiponectin determines farnesoid X receptor agonism-mediated cardioprotection against post-infarction remodelling and dysfunction. Cardiovascular research **114**, 1335–1349 (2018).
51. Yan W, *et al.* N-Cadherin Overexpression Mobilizes the Protective Effects of Mesenchymal Stromal Cells Against Ischemic Heart Injury Through a β-Catenin-Dependent Manner. Circulation research **126**, 857–874 (2020).
52. Li Y, *et al.* S100a8/a9 Signaling Causes Mitochondrial Dysfunction and Cardiomyocyte Death in Response to Ischemic/Reperfusion Injury. Circulation **140**, 751–764 (2019).
53. Li Y, *et al.* Cardiac Fibroblast-Specific Activating Transcription Factor 3 Protects Against Heart Failure by Suppressing MAP2K3-p38 Signaling. Circulation **135**, 2041–2057 (2017).

# table

**Table 1. Mass spectrum analysis of βII spectrin-interacting complex I subunits.**

| Protein name | MS score | Unique peptides | Abundance | Molecular mass (kDa) |
|---|---|---|---|---|
| Ndufa5 | 54.1 | 19 | 7.57E+06 | 13.36 |
| Ndufb7 | 62.6 | 14 | 1.33E+07 | 16.331 |
| Ndufb3 | 54.46 | 17 | 1.06E+07 | 11.692 |
| Ndufs1 | 221.36 | 42 | 2.16E+08 | 79.777 |
| Ndufv1 | 211.67 | 38 | 1.17E+08 | 49.913 |
| Ndufb9 | 172.03 | 46 | 4.36E+07 | 21.984 |
| Ndufa8 | 167.12 | 56 | 8.82E+07 | 19.992 |
| Ndufs2 | 148.98 | 25 | 7.52E+07 | 52.626 |
| Ndufv2 | 148.07 | 27 | 8.33E+07 | 27.285 |
| Ndufs3 | 143.32 | 25 | 5.35E+07 | 30.149 |
| Ndufb10 | 141.01 | 32 | 3.89E+07 | 21.024 |
| Ndufs7 | 139.41 | 31 | 3.43E+07 | 24.683 |
| Ndufa12 | 136.26 | 57 | 2.08E+07 | 17.086 |
| Ndufb4 | 117.31 | 47 | 3.93E+07 | 15.081 |
| Ndufa10 | 112.5 | 15 | 1.98E+07 | 40.603 |
| Ndufa4 | 111.06 | 55 | 4.86E+07 | 9.327 |
| Ndufa6 | 106.42 | 37 | 1.86E+07 | 15.283 |
| Ndufb5 | 99.8 | 27 | 1.95E+07 | 21.71 |
| Ndufb8 | 99.57 | 19 | 1.88E+07 | 21.876 |
| Ndufa9 | 97.03 | 12 | 1.69E+07 | 42.122 |
| Ndufc2 | 96.39 | 24 | 2.00E+07 | 14.164 |
| Ndufab1 | 94.04 | 30 | 1.51E+07 | 14.309 |
| Ndufa13 | 93.72 | 28 | 3.28E+07 | 16.86 |
| Ndufs6 | 82.59 | 28 | 7.93E+06 | 13.02 |
| Ndufs4 | 74.91 | 15 | 5.40E+06 | 19.785 |
| Ndufb6 | 66.87 | 26 | 1.55E+07 | 15.515 |
| Ndufs5 | 63.84 | 32 | 1.29E+07 | 12.648 |
| Ndufs8 | 30.39 | 3 | 2.99E+06 | 24.038 |
| Ndufb11 | 25.47 | 7 | 1.56E+07 | 17.444 |
| ND3 | 21.01 | 6 | 4.00E+06 | 13.219 |

| | | | | |
|---|---|---|---|---|
| Ndufa7 | 20.45 | 12 | 7.27E+06 | 12.576 |

# Figures

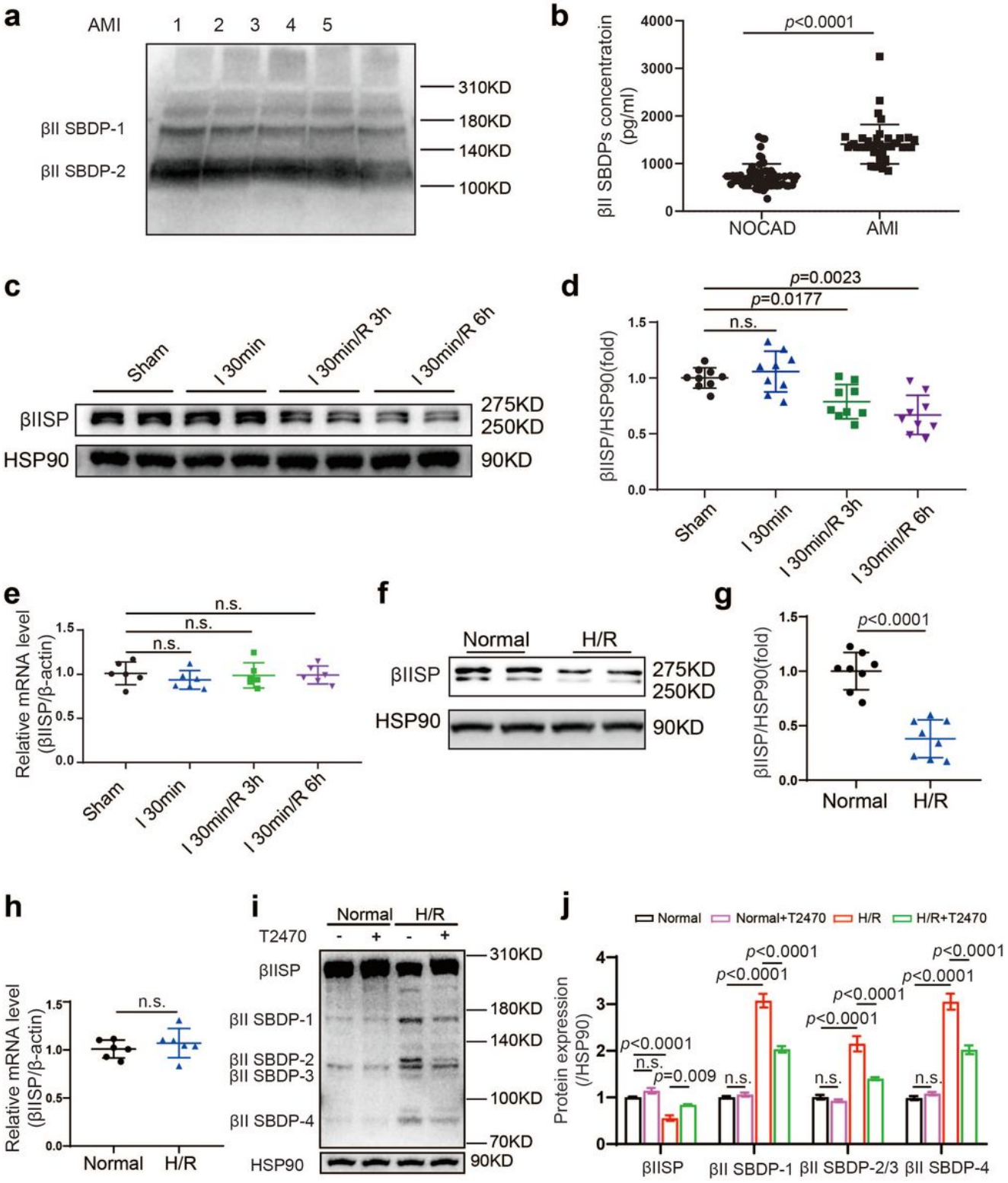


Figure 1

**βII spectrin protein is degraded into βII SBDPs by calpain in the heart during I/R injury**

**a** Western blots of βII SBDPs levels in serum from human AMI patients (n=5). **b** βII SBDPs levels detected by ELISA in serum from NOCAD (n=64) and AMI patients (n=42). **c** and **d** Western blots and quantification of βII spectrin protein levels in sham heart or the infarct border zone of male mouse heart tissues during I/R injury. n=9/group. **e**Real-time PCR analysis of βII spectrin mRNA levels in sham heart or the infarct border zone of male mouse heart tissues during I/R injury. n=6/group. **f** and **g**Western blots and quantification of βII spectrin protein levels in NCMs subjected to normal conditions or 4 hours of hypoxia and 2 hours of reoxygenation (H/R) treatment. n=8/group. **h** Real-time PCR analysis of βII spectrinmRNA levels in NCMs under normal or H/R treatment. n=6/group. **i** and **j** Western blots and quantification of βII spectrin and βII SPDPs levels in NCMs following H/R treatment with or without a calpain inhibitor (T2470, 100 μM). n=3/group. The data are presented as the mean ± SD. Data in **b, g** and **h** were analyzed via unpaired, 2-tailed Student's t test. Data in **d** and **e** were analyzed via one-way ANOVA, followed by Dunnett's post-hoc test. Other data were analyzed via one-way ANOVA, followed by Tukey's post-hoc test. n.s., nonsignificant; AMI, acute myocardial infarction; βII SBDPs, βII spectrin breakdown products; βIISP, βII spectrin; ELISA, enzyme-linked immunosorbent assay; HSP90, heat shock protein 90; I/R, ischemia/reperfusion; H/R, hypoxia/reoxygenation; NCMs, neonatal mouse cardiomyocytes; NOCAD, non-obstructive coronary artery disease.

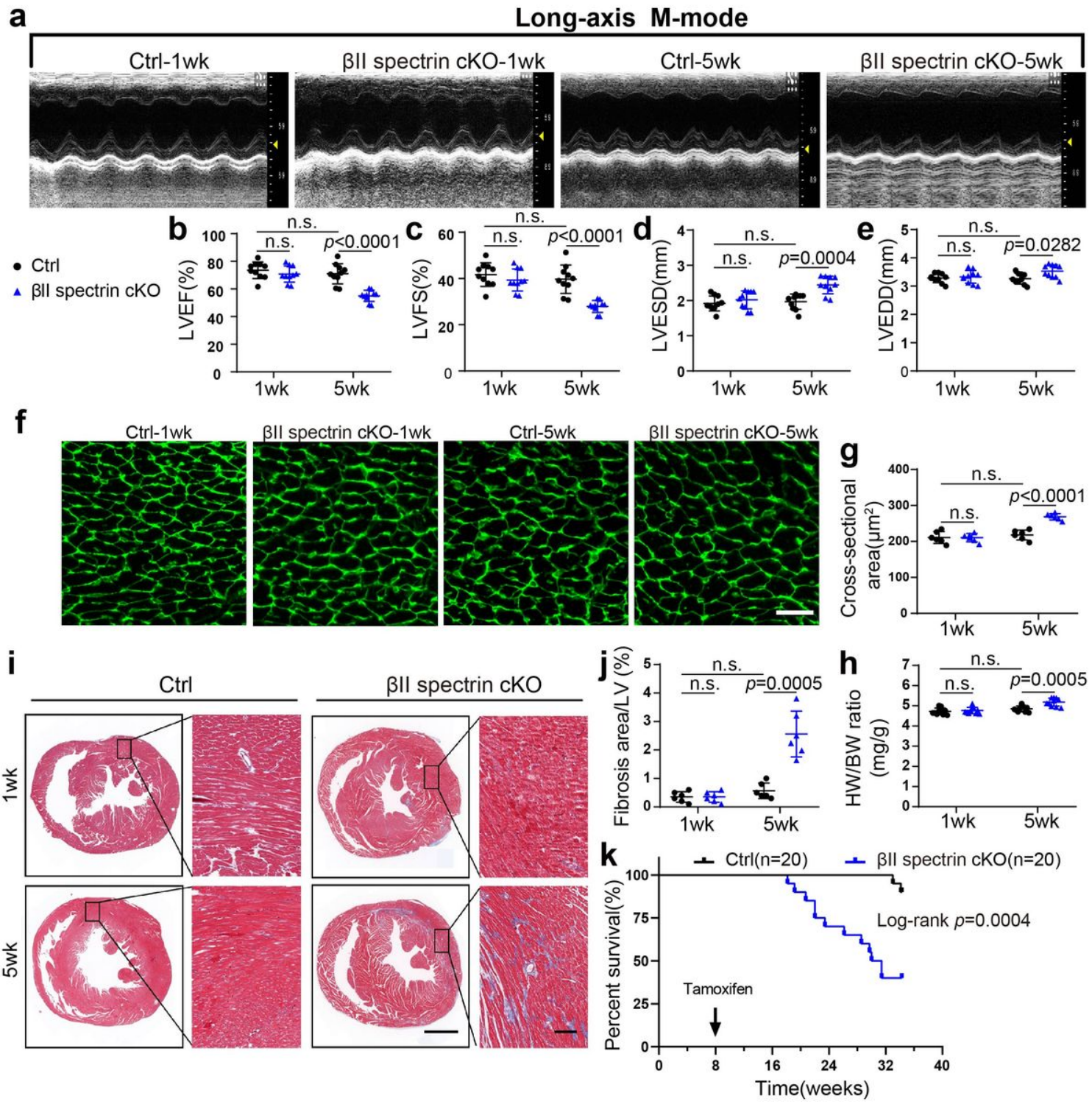


## Figure 2

### Cardiac-specific βII spectrin deficiency in adult mice results in contractile dysfunction, cardiac hypertrophy and fibrosis

**a**Representative long-axis M-mode echocardiography images (scale bar: 0.1 s) and corresponding values for LVEF (**b**), LVFS (**c**), LVESD (**d**) and LVEDD (**e**) in male control (Ctrl) and βII spectrin cKO mice 1 week or 5 weeks after tamoxifen treatment. n=10/group. **f** and **g**Representative microscopy of

immunohistochemical staining for wheat germ agglutinin (WGA, green) and quantification of its cross-sectional area in male Ctrl and βII spectrin cKO mice 1 week or 5 weeks after tamoxifen treatment. Scale bars: 25 μm. n=6/group. **h** Ratios of heart weight to body weight of male Ctrl and βII spectrin cKO mice 1 week or 5 weeks after tamoxifen treatment. n=6/group. **i** and **j** Representative images of heart sections stained with Masson trichrome and quantification of the fibrotic areas in male Ctrl and βII spectrin cKO mice 1 week or 5 weeks after tamoxifen treatment. Scale bars: 3 mm (**right**) and 100 μm (**left**). n=6/group. **k** Postnatal survival curve for male Ctrl(n=20) and βII spectrin cKO mice (n=20). The data are presented as the mean ± SD. Data in **k** were analyzed via Log-rank Mantel-Cox testing. Other data were analyzed via one-way ANOVA, followed by Tukey's post-hoc test. n.s., nonsignificant; BW, body weight; cKO, cardiac knockout; HW, heart weight; LV, left ventricle; LVEDD, left ventricular end-diastolic diameter; LVEF, left ventricular ejection fraction; LVESD, left ventricular end-systolic diameter; LVFS, left ventricular fractional shortening; 1 wk, 1 week; 5 wk, 5 weeks.

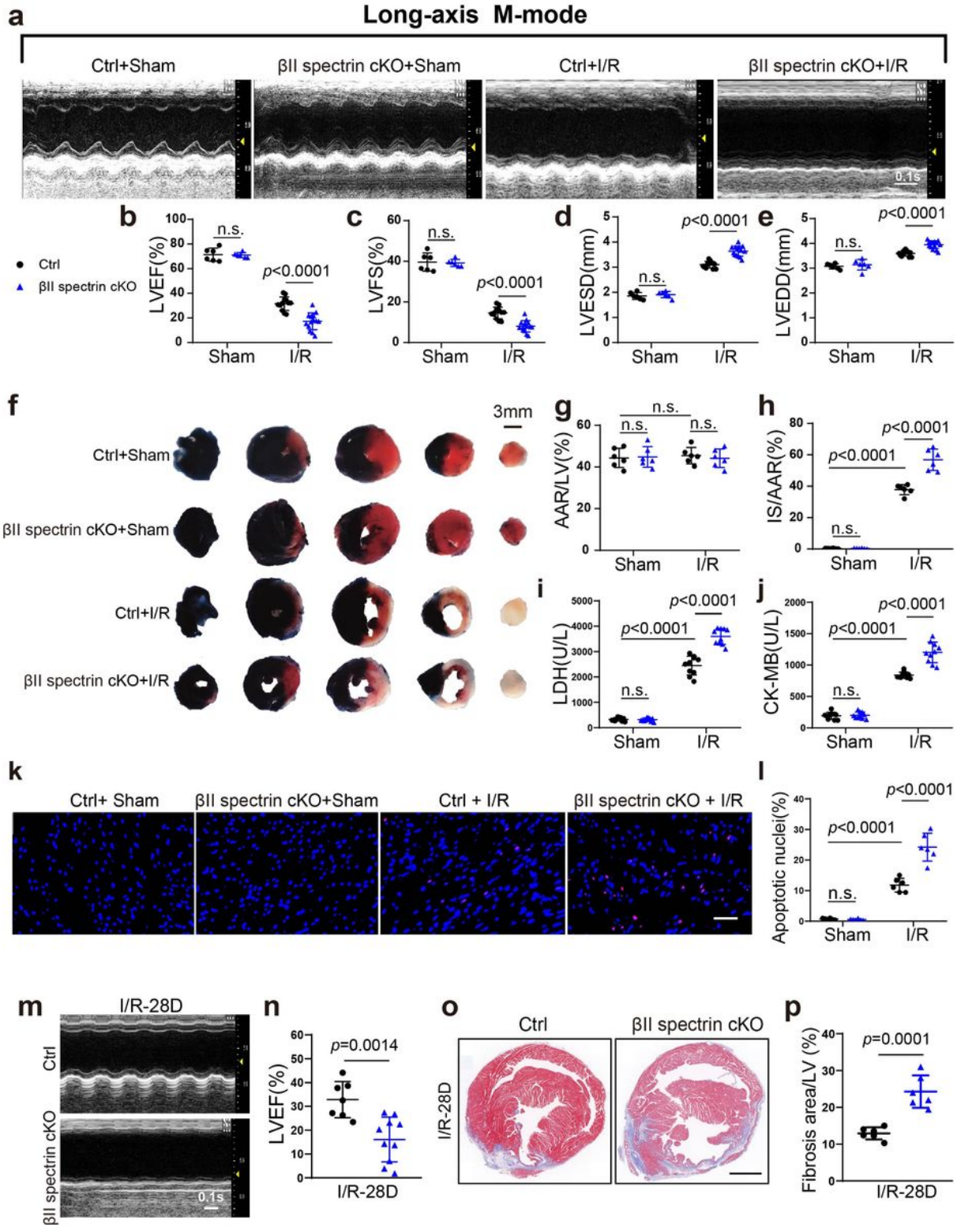


## Figure 3

### Cardiac-specific βII spectrin deficiency in adult mice exacerbates I/R injury

**a**Representative long-axis M-mode echocardiographyimages (scale bar: 0.1 s) and corresponding values for LVEF (**b**), LVFS (**c**), LVESD (**d**) and LVEDD (**e**) in male Ctrl and βII spectrin (βIISP) cKO mice 1 day after sham surgery or I/R. n=6 to 14/group. **f-h** Representative images of Evans blue and triphenyltetrazolium

chloride (TTC) staining and assessment of the area at risk (AAR)/left ventricle (LV) and infarct size (IS)/AAR for hearts from male Ctrl and βII spectrin cKO mice 1 day after sham surgery or I/R. The blue area represents unaffected heart tissue; the white area, infarcted tissue; the red plus white area, tissue at risk. Scale bar: 3 mm. n=6/group. **i** and **j** Serum LDH and CK-MB concentrations in male Ctrl and βII spectrin cKO mice 1 day after sham surgery or I/R. n=6/group. **k** and **l** Representative images and averaged data for TUNEL staining of cardiac sections from male Ctrl and βII spectrin cKO mice 1 day after sham surgery or I/R. Scale bar: 50 μm. n=10/group. **m** and **n** Representative long-axis M-mode echocardiography images (scale bar: 0.1 s) and corresponding values for LVEF 28 days in male Ctrl and βII spectrin cKO mice after I/R injury. n=7 to 10/group. **o** and **p** Representative images of heart sections stained with Masson trichrome and quantification of the fibrotic areas in male Ctrl and βII spectrin cKO mice 28 days after I/R injury. Scale bars: 3 mm. n=6/group. The data are presented as the mean ± SD. Data in **n** and **p** were analyzed via unpaired, 2-tailed Student's t test. Other data were analyzed via one-way ANOVA, followed by Tukey's post-hoc test. n.s., nonsignificant; Cle. caspase 3, cleaved caspase 3; cKO, cardiac knockout; CK-MB, creatine kinase-MB; I/R, ischemia/reperfusion; I/R-28D, 28 days post-I/R; LDH, lactate dehydrogenase; LV, left ventricle; LVEDD, left ventricular end-diastolic diameter; LVEF, left ventricular ejection fraction; LVESD, left ventricular end-systolic diameter; LVFS, left ventricular fractional shortening; TUNEL, terminal deoxynucleotide transferase dUTP nick end labeling.

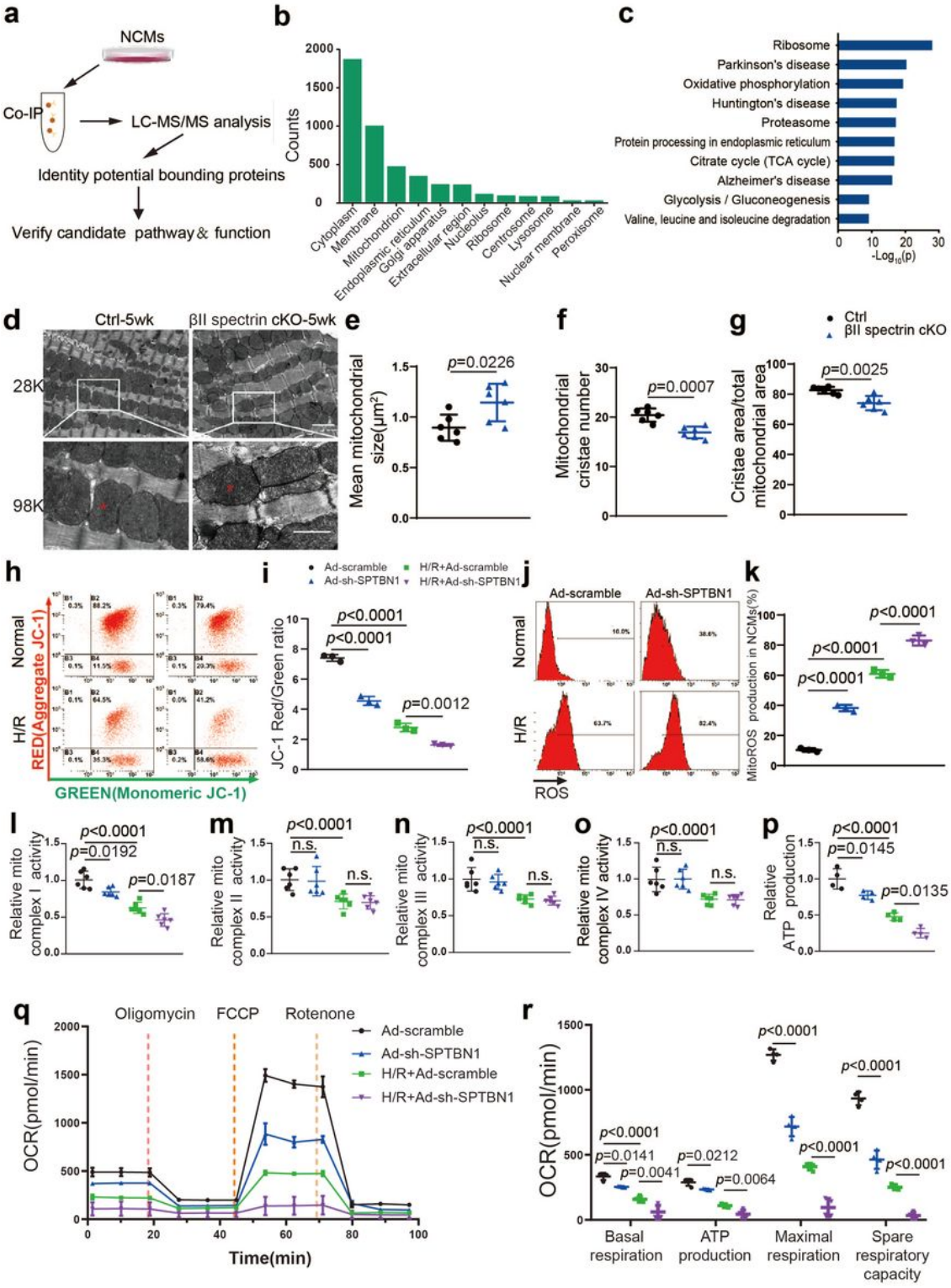


## Figure 4

### Cardiac-specific loss of βII spectrin inhibits mitochondrial complex I and respiratory function

**a** Schematic representation of the experimental protocol. **b** Cellular component analysis of the potential βII spectrin-binding proteins identified by IP–LC–MS/MS using the Gene Ontology (GO) database. **c** The top ten enriched potential βII spectrin-binding proteins in KEGG pathway analysis. **d-g** Representative

transmission electron microscopy images of myocardial mitochondria and quantitative analysis of the mitochondrial size (**e**), cristae number (**f**) and cristae area (**g**) in male Ctrl and βII spectrin cKO mice 5 weeks after tamoxifen treatment (magnification: × 28,000 [28K] and × 98,000 [98K]). Scale bars: 2 μm (**top**) and 1 μm (**bottom**). n=6/group. **h–k** Flow cytometry analysis and quantification of mitochondrial membrane potential after JC-1 staining (**h** and **i**) and flow cytometry analysis and quantification of mitochondria-derived superoxide production after MitoSOX staining (**j** and **k**) in control (Ad-scramble) or βII spectrin-knockdown (Ad-sh-SPTBN1) NCMs under normal or H/R conditions. n=3/group. **l–o** Activity of ETC complexes I (**l**), II (**m**), III (**n**) and IV (**o**) in mitochondrial fractions isolated from control or βII spectrin-knockdown NCMs under normal or H/R conditions. n=6/group. **p** ATP levels in control or βII spectrin-knockdown NCMs under normal or H/R conditions. n=4/group. **q** and **r** The oxygen consumption rate (OCR) and associated quantitative traits in control or βII spectrin-knockdown NCMs under normal or H/R conditions, including basal respiration, ATP production, maximal respiration and spare respiratory capacity. n=4/group. The data are presented as the mean ± SD. Data in **e–g** were analyzed via unpaired, 2-tailed Student's t test. Other data were analyzed via one-way ANOVA, followed by Tukey's post-hoc test. n.s., nonsignificant; co-IP, coimmunoprecipitation; FCCP, carbonyl cyanide-4 (trifluoromethoxy) phenylhydrazone; H/R, hypoxia/reoxygenation; LC–MS/MS, liquid chromatography tandem mass spectrometry; NCMs,neonatal mouse cardiomyocytes; 1 wk, 1 week; 5 wk, 5 weeks.

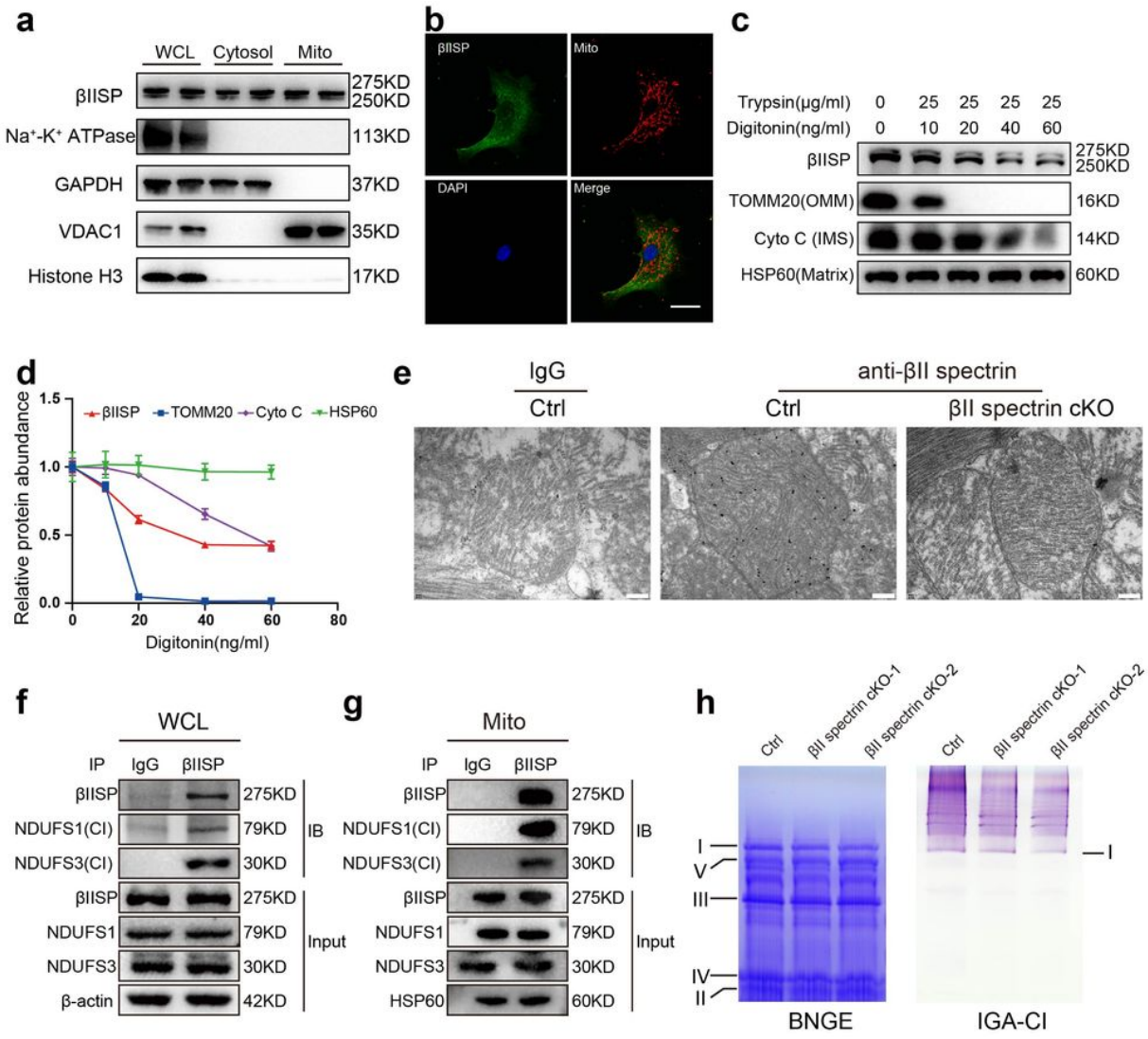


## Figure 5

### βII spectrin interacts with mitochondrial complex I to mediate its assembly in cardiomyocytes

**a** Western blots of βII spectrin expression in the whole-cell, cytosol and mitochondria lysates of NCMs. **b** Representative images of immunofluorescence staining for βII spectrin (green) and mitochondria (red) and DAPI (blue) staining in NCMs. Scale bar: 20 μm. **c** Western blot analysis of the trypsin protection assay of mitochondria derived from NCMs. TOMM20, Cyto C and HSP60 are shown as markers of the outer mitochondrial membrane (OMM), intermembrane space (IMS) and mitochondrial matrix, respectively. The blots were processed in parallel with samples derived from the same experiment. **d** Relative protein abundances in trypsin-digested mitochondria derived from the band intensities of intact proteins quantified from (**c**). **e** Representative immunoelectron microscopy images showing gold-marked βII spectrin particles in myocardial mitochondria from male Ctrl or βII spectrin cKO mice. Scale bar: 200 nm. **f** Coimmunoprecipitation (IP) and immunoblot (IB) analysis of NDUFS1 and NDUFS3 with βII spectrin in NCM whole-cell lysates. **g** Coimmunoprecipitation (IP) and immunoblot (IB) analysis of NDUFS1 and NDUFS3 with βII spectrin in NCM mitochondrial lysates. **h** Blue native gel electrophoresis (BNGE) (**left**) of the indicated ETC assembly and in-gel assays (IGA) (**right**) of the indicated mitochondrial complex I

activity of digitonin-solubilized isolated mitochondria from male Ctrl or βII spectrin cKO mice 5 weeks after tamoxifen treatment. The data are presented as the mean ± SD. n=3/group. βIISP, βII spectrin; cKO, cardiac knockout; CI, mitochondrial complex I; Cyt C, cytochrome c; DAPI, 4',6-diamidino-2-phenylindole; HSP60, heat shock protein 60; Mito, mitochondria; NDUFS1, NADH:ubiquinone oxidoreductase subunit S1; NDUFS3, NADH:ubiquinone oxidoreductase subunit S3; TOMM20, mitochondrial 20 kDa outer membrane protein; WCL, whole-cell lysates.

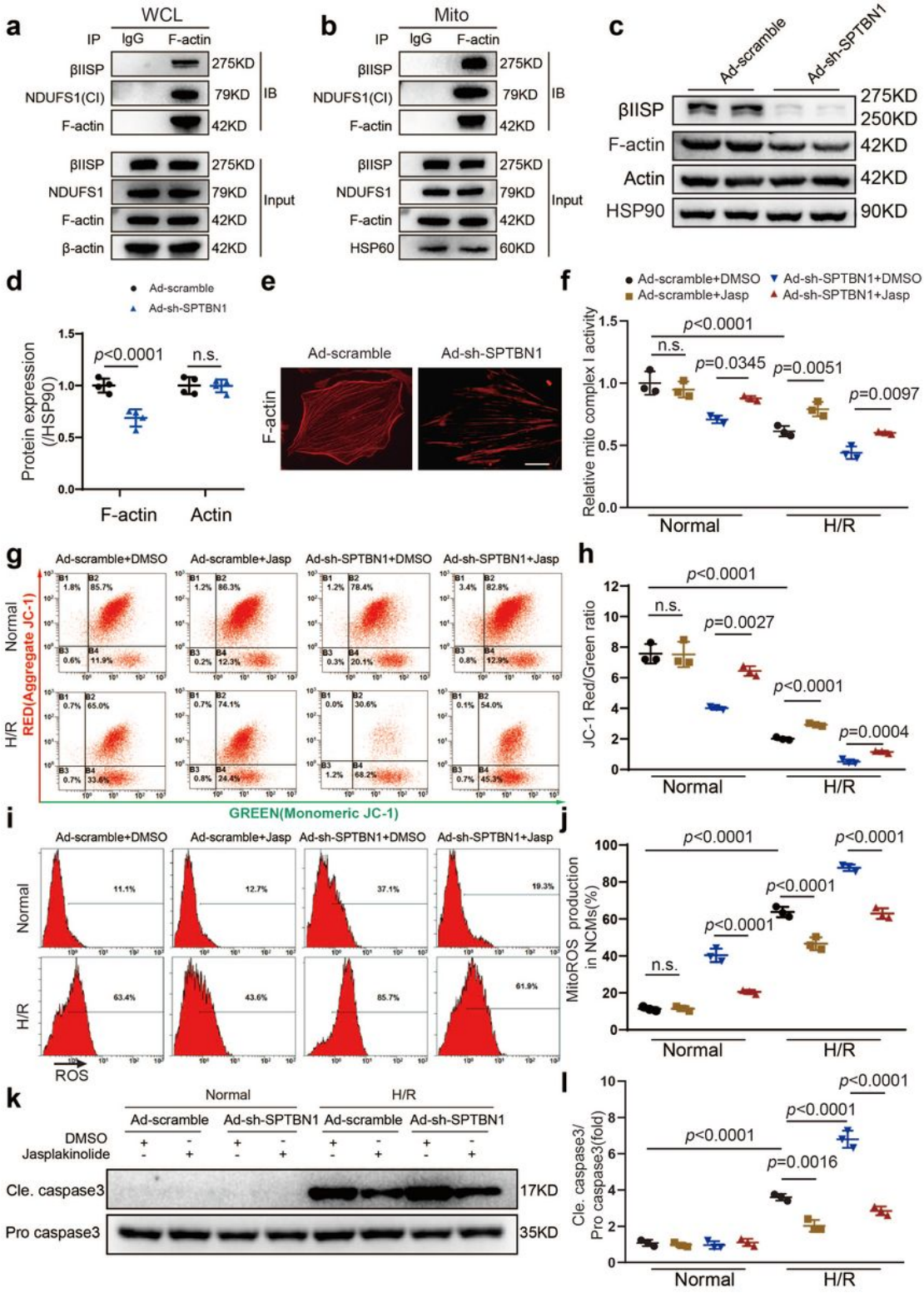

## Figure 6

### βII spectrin regulates complex I activity, mitochondrial function and cardiomyocyte survival by stabilizing F-actin

**a**,Coimmunoprecipitation (IP) and immunoblot (IB) analysis of NDUFS1 and βII spectrin with F-actin in NCM whole-cell lysates. **b** Coimmunoprecipitation (IP) and immunoblot (IB) analysis of NDUFS1 and NDUFS3 with βII spectrin in NCM mitochondrial lysates. **c** Western blots and quantification of βII spectrin, F-actin and total actin expression in control or βII spectrin knockdown NCMs under normal conditions. n=4/group. **e** Confocal fluorescence images showing the organization of F-actin in control or βII spectrin-knockdown NCMs under normal conditions. Scale bar: 20 μm. n=3/group. **f** Activity of ETC complex I in mitochondrial fractions isolated from control or βII spectrin-knockdown NCMs treated with DMSO or jasplakinolide (Jasp, 50 nM), followed by normal or H/R conditions. n=3/group. **g-j** Flow cytometry analysis and quantification of mitochondrial membrane potential after JC-1 staining (**g** and **h**), and flow cytometry analysis and quantification of mitochondria-derived superoxide production after MitoSOX staining (**i** and **j**) in control or βII spectrin-knockdown NCMs treated with DMSO or jasplakinolide (Jasp, 50 nM), followed by normal or H/R conditions. n=3/group. **k** and **l** Western blots of cleaved and pro caspase3 expression in control or βII spectrin-knockdown NCMs treated with DMSO or jasplakinolide (Jasp, 50 nM), followed by normal or H/R conditions. n=3/group. The data are presented as the mean ± SD. Data in d were analyzed via unpaired, 2-tailed Student's t test. Other data were analyzed via one-way ANOVA, followed by Tukey's post-hoc test. n.s., nonsignificant; βIISP, βII spectrin; Cle. caspase 3, cleaved caspase 3; DMSO, dimethylsulfoxide;HSP90, heat shock protein 90; H/R, hypoxia/reoxygenation;WCL, whole-cell lysates.

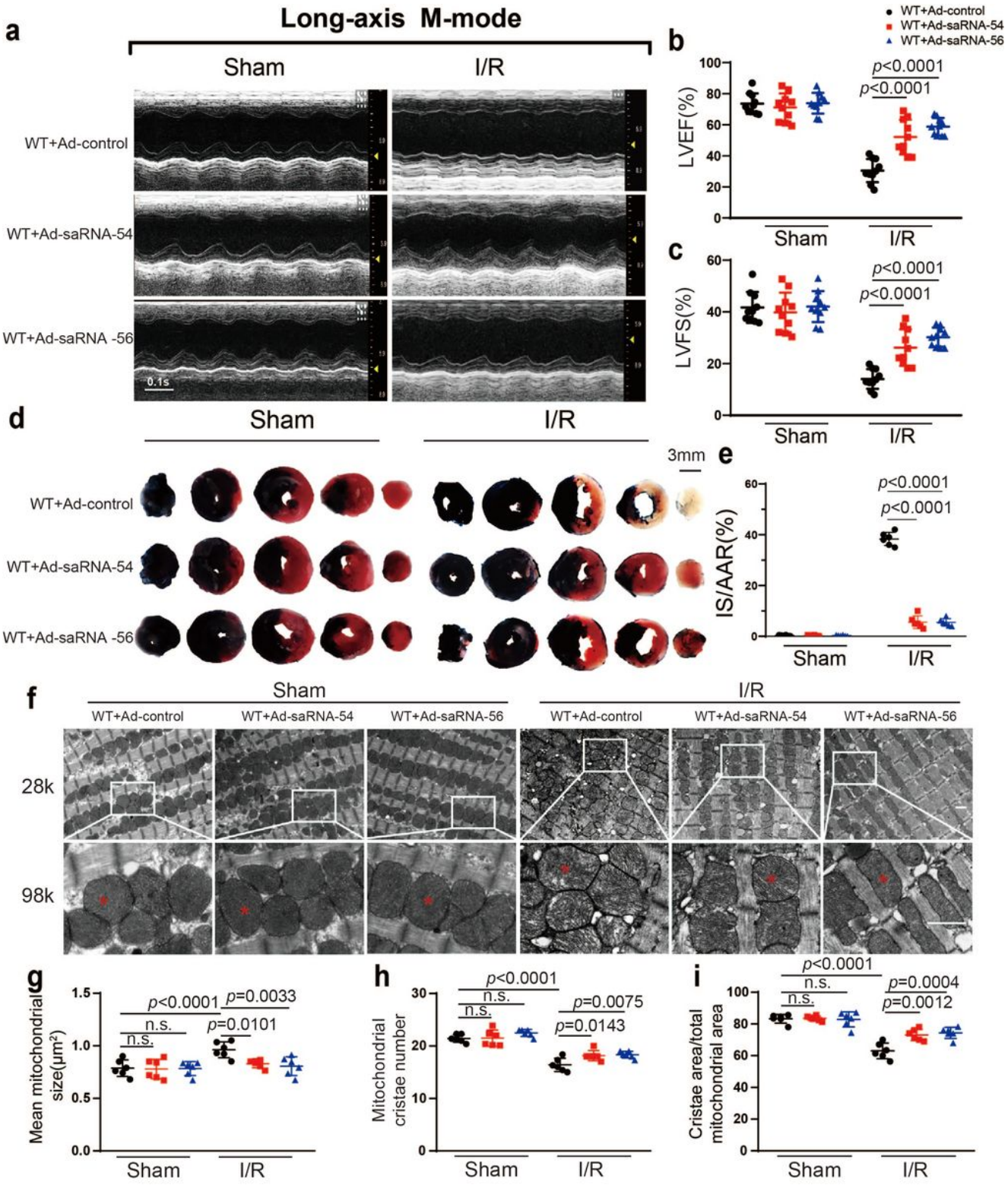


## Figure 7

### βII spectrin overexpression via saRNA inthe heart alleviates I/R injury

**a-c** Representative long-axis M-mode echocardiography images (scale bar: 0.1 s) and corresponding values forLVEF (**b**) and LVFS (**c**) in male sham or I/R-treated mice intramyocardially injected with adenoviruses expressing βII spectrin saRNA (Ad-saRNA-54 or Ad-saRNA-56) or a control sequence (Ad-

control). n=9 to 13/group. **d** and **e** Representative images of Evans blue and triphenyltetrazolium chloride (TTC) staining (scale bar: 3 mm) in hearts and assessment of IS (%AAR)in male sham or I/R-treated mice intramyocardially injected with adenoviruses expressing βII spectrin saRNA (Ad-saRNA-54 or Ad-saRNA-56) or a control sequence (Ad-control). n=6/group. **f-i** Representative transmission electron microscopy images of myocardial mitochondria (magnification: × 28,000 [28K] and × 98,000 [98K]); scale bars (**top** and **bottom**): 1 μm and quantitative analysis of the mitochondrial size (**g**), cristae number (**h**) and cristae area (**i**) in male sham or I/R-treated mice intramyocardially injected with adenoviruses expressing βII spectrin saRNA (Ad-saRNA-54 or Ad-saRNA-56) or a control sequence (Ad-control). n=6/group. The data are presented as the mean ± SD. The data were analyzed via one-way ANOVA, followed by Tukey'spost-hoc test. n.s., nonsignificant; AAR, area at risk;I/R, ischemia/reperfusion; IS, infarct size; LV, left ventricle; LVEDD, left ventricular end-diastolic diameter; LVEF, left ventricular ejection fraction; LVESD, left ventricular end-systolic diameter; LVFS, left ventricular fractional shortening; WT, wild type.

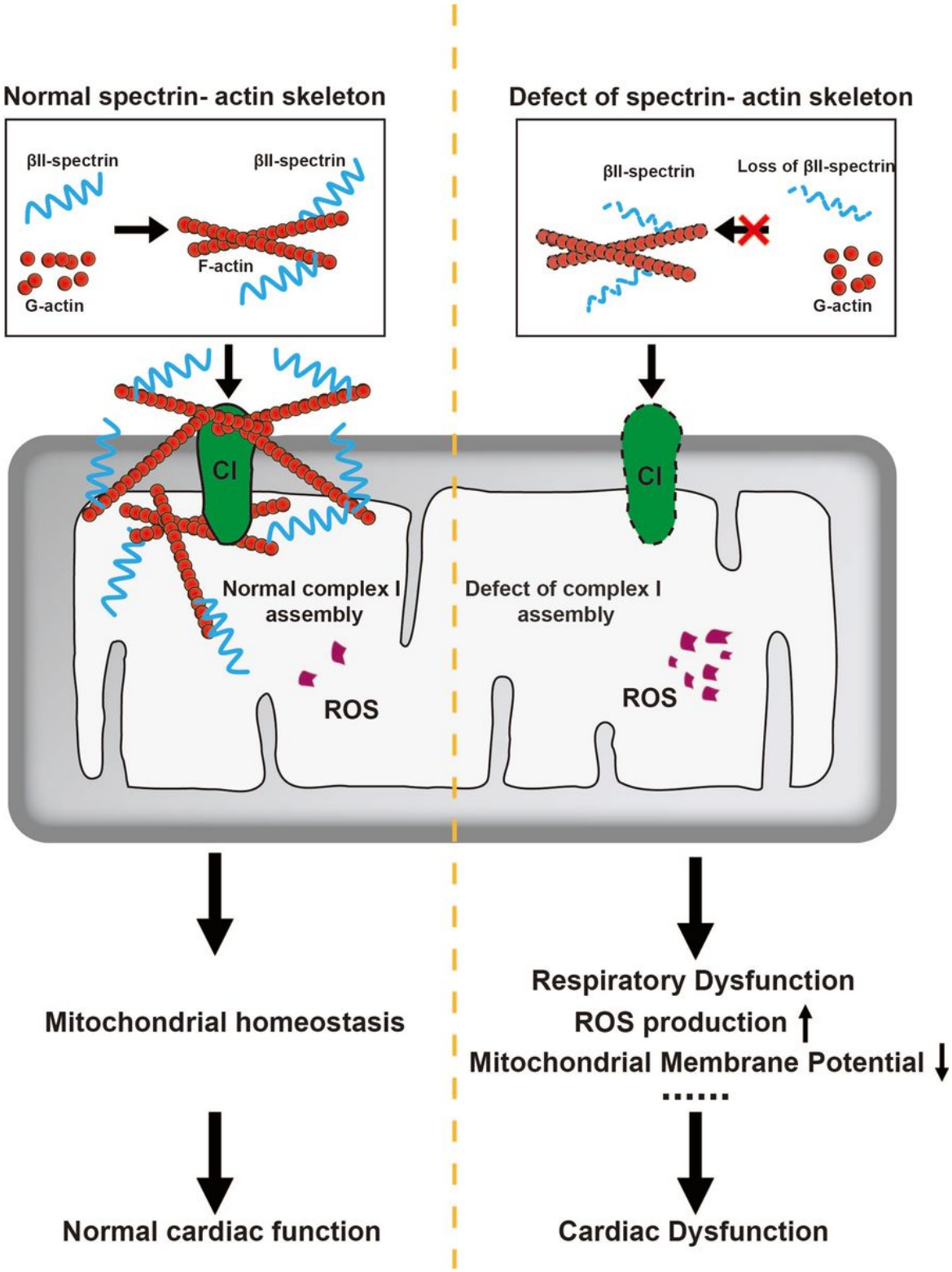


Figure 8

**Summary figure**: Cardiomyocyte βII spectrin crosslinks with F-actin to form spectrin-actin cytoskeleton that interacts with mitochondrial complex I to mediate its assembly. Without βII spectrin, cardiomyocyte mitochondrial function deteriorates due to defects incomplex I assembly, resulting in cardiac dysfunction.

# Supplementary Files

This is a list of supplementary files associated with this preprint. Click to download.

- SupplementalMaterials.docx
- FullunEditedWesternblots.pdf